

# Structures and Energies of Coadsorbed CO and H<sub>2</sub> on Fe<sub>5</sub>C<sub>2</sub>(001), Fe<sub>5</sub>C<sub>2</sub>(110), and Fe<sub>5</sub>C<sub>2</sub>(100)

Dong-Bo Cao,<sup>†</sup> Fu-Qiang Zhang,<sup>†</sup> Yong-Wang Li,<sup>†</sup> Jianguo Wang,<sup>†</sup> and Haijun Jiao<sup>\*,†,‡</sup>

State Key Laboratory of Coal Conversion, Institute of Coal Chemistry, Chinese Academy of Sciences, Taiyuan 030001, People's Republic of China, and Leibniz-Institut für Organische Katalyse an der Universität Rostock e.V., Buchbinderstrasse 5-6, 18055 Rostock, Germany

Received: February 23, 2005; In Final Form: April 8, 2005

Density functional theory calculations have been carried out on the CO/H<sub>2</sub> coadsorption on the (001), (110), and (100) surfaces of Fe<sub>5</sub>C<sub>2</sub> for the understanding of the Fischer–Tropsch synthesis (FTS) mechanism. The stable surface species changes with the variation of the H<sub>2</sub> and CO coverage. Along with dissociated hydrogen and adsorbed CO in 2-, 3-, and 4-fold configurations, methylidyne (C<sub>s</sub>H) (C<sub>s</sub>, surface carbon), ketenylidene (C<sub>s</sub>CO), ketenyl (C<sub>s</sub>HCO), ketene (C<sub>s</sub>H<sub>2</sub>CO), and carbon suboxide (C<sub>s</sub>C<sub>2</sub>O<sub>2</sub>) are computed as thermodynamically stable surface species on Fe<sub>5</sub>C<sub>2</sub>(001) and Fe<sub>5</sub>C<sub>2</sub>(110) containing both surface iron and carbon atoms. These surface carbon species can be considered as the preliminary stages for FTS. On Fe<sub>5</sub>C<sub>2</sub>(100) with only iron atoms on the surface layer, the stable surface species is dissociated hydrogen and CO with top and 2-fold configurations. The bonding nature of these adsorbed carbon species has been analyzed.

## 1. Introduction

Iron-based catalysts are widely used in the industrial Fischer–Tropsch synthesis (FTS) processes for converting CO and H<sub>2</sub> into high-quality liquid fuels.<sup>1</sup> In the course of FTS reactions, iron-based catalysts are naturally exposed to the syngas (CO and H<sub>2</sub> mixture) environment that maintains the stability of the active iron carbide phases. Among many coexisting types of carbides as catalysts, Hägg iron carbide (Fe<sub>5</sub>C<sub>2</sub>) is the most representative one.<sup>2</sup> Different C<sub>x</sub>H<sub>y</sub> species on the Fe(110) surfaces have been proposed by Erley et al.<sup>3</sup> on the basis of high-resolution electron energy loss spectroscopy (HREELS). However, it should be noted that it is experimentally difficult to determine even the initial states (surface species) over an iron-based catalyst under FTS conditions, which are essential to understand the mechanism and FTS kinetics in detail.

Coadsorption of CO and H<sub>2</sub> on transition metal surfaces is of technological importance to catalysts<sup>4–11</sup> and fuel cells.<sup>12–14</sup> Coadsorption of CO and H<sub>2</sub> on transition metal surfaces has widely been studied, for example, on the surfaces of Ni(110),<sup>4</sup> Ni(100),<sup>5</sup> Fe(111),<sup>6</sup> Fe(100),<sup>7</sup> Rh(100),<sup>8</sup> Gd(0001),<sup>9</sup> Pd(111),<sup>10</sup> Pt(111),<sup>11</sup> Pt(335),<sup>12</sup> Pt(112),<sup>13</sup> and bimetallic PtRu.<sup>14</sup> Experimental investigations of the coadsorption of CO and H<sub>2</sub> on Cu<sub>3</sub>Pt(111)<sup>15</sup> and Ni(110)<sup>4</sup> revealed a local repulsive interaction between hydrogen and CO. A theoretical study on the coadsorption of CO and H<sub>2</sub> on Ni(100) showed that the CO and H interaction depopulates the 2π\* state of CO and strengthens the C–O bond.<sup>5a</sup> On the coadsorbed Ni(100) and Ni(111) surfaces, neither C–H nor O–H bonds were detected by thermal desorption experiments.<sup>16</sup> Hydrogen adsorption was inhibited by preadsorbed CO, as found in the temperature-program desorption and low-energy electron-diffraction experiments.<sup>6,7,10,17</sup>

The major difference between Fe<sub>5</sub>C<sub>2</sub> and the above-mentioned metal surfaces is that Fe<sub>5</sub>C<sub>2</sub> has surface carbon atoms. On the Fe<sub>5</sub>C<sub>2</sub>(001) and (110) surfaces, H<sub>2</sub> adsorption forms H, C<sub>s</sub>H (C<sub>s</sub>,

surface carbon), and C<sub>s</sub>H<sub>2</sub> species, and C<sub>s</sub>H is the most stable species at various coverages.<sup>18</sup> A similar phenomenon has been observed in the adsorption–desorption experiments with CO/D<sub>2</sub> and <sup>13</sup>CO/H<sub>2</sub> as reactants.<sup>19</sup> Loggenberg et al. reported the existence of C<sub>2</sub>H<sub>x</sub>O in the reaction of coadsorbed CO and diazomethane (CH<sub>2</sub>N<sub>2</sub>) on an iron surface by X-ray photoelectron spectroscopy.<sup>20</sup> In our previous work, we investigated CO and H<sub>2</sub> respective adsorption on Fe<sub>5</sub>C<sub>2</sub>(001), (110), and (100).<sup>18,21</sup> In this work, we present extensive calculations of the coadsorption of CO and H<sub>2</sub> on the three surfaces of Fe<sub>5</sub>C<sub>2</sub> at different coverages and H<sub>2</sub>/CO ratios, especially the thermodynamic property of the coexisting species on the surfaces. Thermodynamic studies can provide the adsorption energies of various surface species at different coverages and H<sub>2</sub>/CO ratios and the structure and stability of various species, which are important for understanding the initial activation step of FTS. It is found that ketenylidene (C<sub>s</sub>CO), ketenyl (C<sub>s</sub>HCO), ketene (C<sub>s</sub>H<sub>2</sub>CO), and carbon suboxide (C<sub>s</sub>C<sub>2</sub>O<sub>2</sub>) formed by CO and H<sub>2</sub> coadsorption are very interesting due to the presence of the adjacent C=C and C=O bonds. We have also analyzed the bonding nature of these surface species with metal atoms using local density of states (LDOS). Due to the complexity of the orbitals and also the fact that frontier orbitals are important and responsible for the interaction, only the highest occupied and the lowest unoccupied orbitals are used for discussion and the other low-lying occupied orbitals are only shown for comparison.

## 2. Methods and Models

Coadsorption of H<sub>2</sub> and CO on the surfaces of Fe<sub>5</sub>C<sub>2</sub> was studied by density functional theory, as implemented in the Cambridge Sequential Total Energy Package (CASTEP).<sup>22</sup> The exchange correlation energy was described using the Perdew–Burke–Ernzerhof (PBE)<sup>23</sup> form of generalized gradient approximations (GGA). Ionic cores were described by an ultrasoft pseudopotential,<sup>24</sup> and the Kohn–Sham one-electron states were expanded in a plane wave basis set up to 340 eV. A Fermi smearing of 0.1 eV was utilized. Brillouin zone integration was approximated by a sum over special *k*-points chosen using the Monkhorst–Pack scheme.<sup>25</sup> The pseudopotential with a partial

\* Corresponding author. E-mail: hjiao@ifok.uni-rostock.de.

<sup>†</sup> Chinese Academy of Sciences.

<sup>‡</sup> Leibniz-Institut für Organische Katalyse an der Universität Rostock e.V.

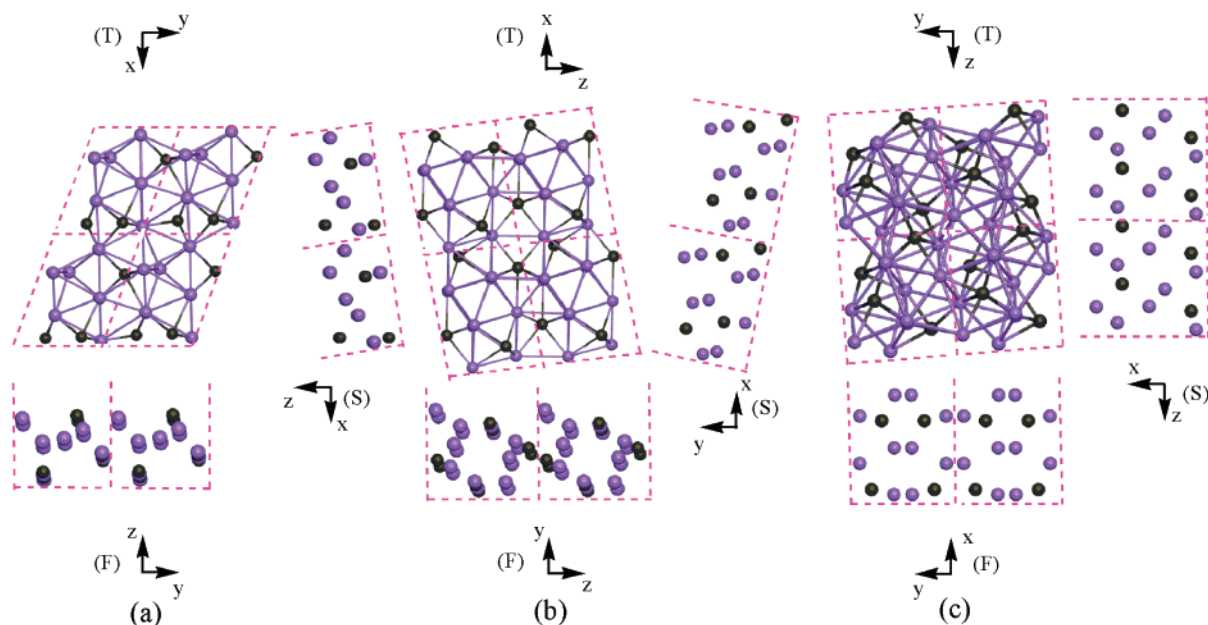


**Figure 1.** Schematic top (T), front (F), and side (S) views of the (001) (a), (110) (b), and (100) (c) surfaces in a  $p(1 \times 1)$  unit cell of  $\text{Fe}_5\text{C}_2$  (purple, Fe atom; gray, C atom).

core was used in spin-polarized calculations to include nonlinear core corrections.<sup>26</sup> Spin polarization having a major effect on the adsorption energies for a magnetic system<sup>27</sup> was included for the super paramagnetic  $\text{Fe}_5\text{C}_2$ <sup>28</sup> to correctly account for its magnetic properties. Spin polarization was also used to calculate the energy and structural parameters of the isolated CHCO species. Without counting the adsorbate, the vacuum between the slabs was set to span in the range of 10 Å to ensure no significant interaction between the slabs. The convergence criteria for structure optimization and energy calculation were set to the following: (a) SCF tolerance of  $2.0 \times 10^{-6}$  eV/atom, (b) energy tolerance of  $2.0 \times 10^{-5}$  eV/atom, (c) maximum force tolerance of 0.05 eV/Å, and (d) maximum displacement tolerance of  $2.0 \times 10^{-3}$  Å. For checking the influence of force, we also performed calculations at a level of maximum force tolerance of 0.03 eV/Å. The resultant change of adsorption energies is very small, for example, 0.002 eV for **1**, **4**, and **7** on  $\text{Fe}_5\text{C}_2(001)$ ; 0.001 and 0.002 eV for **18** and **24** on  $\text{Fe}_5\text{C}_2(110)$ , respectively; and 0.003 and 0.004 eV for **35** and **39** on  $\text{Fe}_5\text{C}_2(100)$ , respectively (see the Results section). We used the Molarch<sup>+</sup> program<sup>29</sup> to generate the molecular graphics.

Hägg iron carbide ( $\text{Fe}_5\text{C}_2$ ) has a monoclinic unit cell ( $a = 11.5620$  Å,  $b = 4.5727$  Å,  $c = 5.0595$  Å, and  $\beta = 97.74^\circ$ ).<sup>21</sup> In our previous work,<sup>18,21</sup> the optimized unit cell parameters agreed with the experimental values ( $a = 11.5007$  Å,  $b = 4.4789$  Å,  $c = 4.9536$  Å, and  $\beta = 97.63^\circ$ ). For the three surfaces of  $\text{Fe}_5\text{C}_2$ , (001), (110), and (100) created from the  $\text{Fe}_5\text{C}_2$  crystal structure, the geometric and energetic differences between the bare and optimized structures are small and reveal the quality of the employed theoretical methods.

For studying the coadsorption of CO and H<sub>2</sub>, it is necessary to consider the adsorption step on the surface. Since CO adsorption on  $\text{Fe}_5\text{C}_2$  is stronger than H<sub>2</sub>, as found in our previous work,<sup>18,21</sup> it is reasonable to consider that CO will adsorb prior to H<sub>2</sub> under a syngas ( $\text{CO} + \text{H}_2$ ) environment. Therefore, coadsorption of H<sub>2</sub> was built up on the model of preadsorbed CO systems.<sup>21</sup> Since the ratio of H<sub>2</sub> to CO lies in the range from 0.5 to 1.7 in a working iron catalyst,<sup>2f,30</sup> the ratio of H<sub>2</sub>/CO as 1/2, 1/1, and 2/1 on (001), (110), and (100) is used in this paper. For a ratio of 1/2 H<sub>2</sub>/CO, the respective coverage of

H<sub>2</sub> and CO is 1/6 and 1/3 monolayer (ML) on  $\text{Fe}_5\text{C}_2(001)$ , 1/6 and 1/3 ML on (110), and 1/4 and 1/2 ML on (100). For a ratio of 1/1 H<sub>2</sub>/CO, the coverage of both H<sub>2</sub> and CO is 1/6 ML on  $\text{Fe}_5\text{C}_2(001)$ , 1/6 ML on (110), and 1/4 ML on (100). For a ratio of 2/1 H<sub>2</sub>/CO, the respective coverage of H<sub>2</sub> and CO is 1/3 and 1/6 ML on (001), 1/3 and 1/6 ML on (110), and 1/2 and 1/4 ML on (100). The initial H<sub>2</sub> was placed at the top, 2-fold site, and 3-fold site of surface iron atoms and at the top of surface carbons. The distances of H<sub>2</sub> and the iron atoms were set to 1.75 Å for H–Fe (from low-energy electronic diffraction<sup>31</sup>) and those for the surface carbon ( $\text{C}_s\text{--H}$ ) to 1.25 Å, while the H–H distance was set to 0.75 Å. All initial orientations, such as top, 2-fold, 3-fold, and 4-fold sites of CO and H<sub>2</sub> on the three surfaces, were considered. Optimization from all initial positions of CO and H<sub>2</sub> coadsorption converges to the same energy minimum structure, and therefore, this minimum structure can also be considered as the most stable structure.

For the side view of  $\text{Fe}_5\text{C}_2(001)$ , we used a model system with five iron layers and three carbon layers (5Fe/3C), in which the bottom two iron layers and two carbon layers (2Fe/2C) were fixed in their bulk positions, while the three iron layers and one carbon layer on the top (3Fe/1C) were allowed to relax (Figure 1a). The top layer of  $\text{Fe}_5\text{C}_2(001)$  has both Fe and C, and their ratio is 1/1, while the second and third layers contain only Fe atoms. A  $3 \times 5 \times 2$   $k$ -grid sampling within the Brillouin zones was used in the  $p(1 \times 1)$  unit cell. For checking the influence of the surface relaxation, we also performed calculations on a model system with seven-layered iron and three-layered carbon atoms (7Fe/3C) under the relaxation of the top four layers of iron and two layers of carbon atoms (4Fe/2C), and the adsorption energy of species **1**, **4**, and **7** changes 0.07, −0.06 and 0.18 eV, respectively (see the Results section).

For the side view of  $\text{Fe}_5\text{C}_2(110)$ , a slab consisting of six iron layers and four carbon layers (6Fe/4C) with a  $p(1 \times 1)$  surface unit cell was modeled (Figure 1b). The top layer is composed of Fe atoms, while the ratio of Fe and C is 2/1 on the second and third layers, and the carbon atoms of the second layer are exposed, setting up the open-surface structure. In the calculations, the bottom three iron layers and two carbon layers (3Fe/2C) were fixed in their bulk positions, while the top three iron

layers and two carbon layers (3Fe/2C) were allowed to relax. A  $k$ -point sampling was performed using  $4 \times 3 \times 1$  Monkhorst–Pack meshes for the unit cell. It is found that a slab of five layers of iron and three layers of carbon atoms (5Fe/3C) under the relaxation of the top three layers of iron and two layers of carbon atoms (3Fe/2C) results in energy changes in species **18** and **24** of 0.10 and  $-0.03$  eV, respectively. A test calculation on a slab of six layers of iron and four layers of carbon atoms (6Fe/4C) under the relaxation of the top four layers of iron and three layers of carbon atoms (4Fe/3C) results in energy changes in species **18** and **24** of 0.02 and  $-0.16$  eV, respectively (see the Results section).

For the side view of Fe<sub>5</sub>C<sub>2</sub>(100), a slab of five iron layers and two carbon layers (5Fe/2C) with a  $p(1 \times 1)$  surface unit cell was modeled (Figure 1c). The top and third layers consist of Fe atoms, while the ratio of Fe and C is 1/1 on the second layer, and the carbon atoms are covered or hidden under the top Fe layer. In the calculations, the bottom two iron layers and one carbon layer (2Fe/1C) were fixed in their bulk positions, while the top three iron layers and one carbon layer (3Fe/1C) were allowed to relax. A  $k$ -point sampling of the  $4 \times 4 \times 1$  Monkhorst–Pack meshes for the unit cell was used. With a slab of four-layered iron and one-layered carbon atoms (4Fe/1C) under the relaxation of the top two-layered iron and one-layered carbon atoms (2Fe/1C), the changes of adsorption energies in species **35** and **39** are  $-0.02$  and  $0.05$  eV (see the Results section). Thus, there is no significant effect of the slab thickness and surface relaxation on the adsorption energy in all surfaces. In our previous work for the adsorption of CO and H<sub>2</sub> on Fe<sub>5</sub>C<sub>2</sub>(001), (110), and (100),<sup>18,21</sup> some tests on  $k$ -point, and cutoff for the adsorption energy have shown no significant change in adsorption energies for using larger surface models.

The linear ketenyl (CHCO) has a doublet ground <sup>2</sup>Π electronic state.<sup>32</sup> The computed C–C and C–O bond lengths of ketenyl are 1.256 and 1.192 Å, respectively. The C=C and C=O bonds lengths of ketene (CH<sub>2</sub>CO) are 1.293 and 1.176 Å, respectively, close to the reported bond lengths (1.32 and 1.16 Å).<sup>33</sup> The C=C and C=O bond lengths of carbon suboxide (C<sub>3</sub>O<sub>2</sub>) are 1.265 and 1.172 Å, in agreement with the experimental values (1.289 and 1.163 Å).<sup>34</sup>

The adsorption energy for  $m$ CO and  $n$ H<sub>2</sub> is defined as the following:  $E_{\text{ads}} = E(m\text{CO}/n\text{H}_2/\text{slab}) - [E(\text{slab}) + E(m\text{CO}) + E(n\text{H}_2)]$ , where  $m$  and  $n$  are the numbers of adsorbed CO and H<sub>2</sub>, respectively,  $E(m\text{CO}/n\text{H}_2/\text{slab})$  is the total energy for the slabs with CO and hydrogen adsorbed on the surface,  $E(\text{slab})$  is the total energy of the bare slab of the surface, and  $E(\text{H}_2)$  and  $E(\text{CO})$  are the total energies of free H<sub>2</sub> and CO. The adsorption energy of surface species, ketenyl (CHCO), ketene (CH<sub>2</sub>CO), and carbon suboxide (C<sub>3</sub>O<sub>2</sub>), was defined as the following:  $E_{\text{ads}} = E(\text{adsorbate}/\text{slab}') - [E(\text{slab}') + E(\text{adsorbate})]$ , where  $E(\text{adsorbate}/\text{slab}')$  is the total energy for the slabs excluding the surface carbon atom with CHCO/CH<sub>2</sub>CO/C<sub>3</sub>O<sub>2</sub> adsorbed on the surface,  $E(\text{slab}')$  is the total energy of the slab excluding the surface carbon atom, and  $E(\text{adsorbate})$  are the total energies of free CHCO or CH<sub>2</sub>CO or C<sub>3</sub>O<sub>2</sub>. Therefore, the more negative the  $E_{\text{ads}}$  value, the higher the adsorption energy.

### 3. Results

**3.1. Coadsorption of CO and H<sub>2</sub> on Fe<sub>5</sub>C<sub>2</sub>(001).** **3.1.1. Structure and Energy.** For the bare Fe<sub>5</sub>C<sub>2</sub>(001) surface with a 1/1 H<sub>2</sub>/CO ratio, the coverage of both CO and H<sub>2</sub> is 1/6 monolayer (ML). As shown in Figure 2, there are eight adsorption forms (**1–8**), and the calculated adsorption energies are listed in Table 1. In **1**, H<sub>2</sub> dissociates and forms surface C<sub>s</sub>H and H, and there are CO, surface C<sub>s</sub>H, and H species. The

**TABLE 1: Computed Bond Lengths ( $d$ , Å) and Adsorption Energies ( $E_{\text{ads}}$ , eV) for CO and H<sub>2</sub> Coadsorption on Fe<sub>5</sub>C<sub>2</sub>(001) with a Coverage of 1/6 ML for Both H<sub>2</sub> and CO (1/1 H<sub>2</sub>/CO)**

composition	$E_{\text{ads}}$	$d_{\text{C-O}}$	$d_{\text{C-Fe}}$	$d_{\text{C-Cs}}$	$d_{\text{O-Fe}}$	$d_{\text{H-Fe}}$		$d_{\text{H-Cs}}$
						a	b	
<b>1</b> CO, H, C <sub>s</sub> H	$-3.09$	1.187	1.780	2.114		1.729		1.094
						1.732		
						1.793		
<b>2</b> CO, C <sub>s</sub> H <sub>2</sub>	$-2.84$	1.201	1.803	2.063		1.688		1.095
<b>3</b> CO, 2H	$-2.31$	1.182	1.814	2.082		1.604	1.668	
						1.764	1.794	
						1.726	1.723	
<b>4</b> C <sub>s</sub> CO, 2H	$-2.91$	1.259	1.978	1.370	2.045	1.721	1.601	
						1.753	1.947	
						1.649	1.627	
<b>5</b> C <sub>s</sub> CO, 2H	$-2.66$	1.247	2.012	1.369	2.231	1.770	1.723	
						1.856	1.776	
<b>6</b> C <sub>s</sub> HCO, H	$-2.76$ ( $-3.87$ ) <sup>a</sup>	1.298	1.914	1.412	2.048	1.673		1.101
						1.762		
						1.925		
<b>7</b> C <sub>s</sub> H <sub>2</sub> CO	$-2.50$ ( $-2.41$ ) <sup>b</sup>	1.359	1.909	1.471	2.033			1.100
						1.986	2.062	
<b>8</b> C <sub>s</sub> H <sub>2</sub> CO	$-2.28$ ( $-2.19$ ) <sup>b</sup>	1.295	1.891	1.473	1.953	1.896		1.097
						2.411		

<sup>a</sup> Using CHCO as adsorbate. <sup>b</sup> Using CH<sub>2</sub>CO as adsorbate.

adsorption energy of **1** is  $-3.09$  eV, and it is the highest among all eight forms. In **2**, there is surface C<sub>s</sub>H<sub>2</sub> formed and CO. One H of C<sub>s</sub>H<sub>2</sub> in **2** interacts agostically with the neighbor iron atom by 1.243 Å for C<sub>s</sub>–H and 1.688 Å for Fe–H, and the adsorption energy is  $-2.84$  eV. **3** consists of CO and H species, and the adsorption energy is  $-2.31$  eV. In **1–3**, the adsorbed CO interacts only with surface iron, and the adsorbed H interacts with both surface iron and carbon. However, there is no direct interaction between the adsorbed CO and H at 1/6 ML.

In **4** and **5**, the adsorbed CO interacts with both surface iron and carbon, resulting in the formation of the adsorbed surface ketenylidene species (C<sub>s</sub>CO), while H<sub>2</sub> is dissociated, and the formed atomic hydrogen interacts with surface iron at 3-fold sites. The adsorption energies of **4** and **5** are  $-2.91$  and  $-2.66$  eV, respectively.

In **6**, both adsorbed CO and H interact with surface iron and carbon, resulting in the formation of an adsorbed ketenyl unit (C<sub>s</sub>HCO) on the surface. The C–C and C–O bond lengths are 1.412 and 1.298 Å, and those of free ketenyl at the same level are 1.256 and 1.192 Å, respectively. The Fe–O bond length in **6** is 2.048 Å. Taking CO and H<sub>2</sub> as adsorbates, the adsorption energy is  $-2.76$  eV, while the adsorption energy is  $-3.87$  eV for taking surface C<sub>s</sub>HCO as adsorbate.

Similar to **6** in the interaction between surface atoms (Fe and/or C) and the adsorbed CO and H, surface ketene (C<sub>s</sub>H<sub>2</sub>CO) is formed in **7** and **8**. The C–C and C–O bond lengths are 1.471 and 1.359 in **7** and 1.473 and 1.295 Å in **8**, which are longer than those in free ketene (1.293 and 1.176 Å). As shown in Figure 2, the two carbon atoms in C<sub>s</sub>H<sub>2</sub>CO interact with iron atoms, and the Fe–O bond lengths are 2.033 and 2.062 Å in **7** and 1.953 Å in **8**. One of the C–H bonds of the C<sub>s</sub>H<sub>2</sub> unit in **8** interacts agostically with the neighbor iron atom by 1.145 Å for C–H and 1.896 Å for Fe–H. These interactions result in a  $\eta^3$  (C=C=O) coordination form on the surface, and this structure pattern is in agreement with that derived from the HREELS analysis for ketene adsorption on the Ru(001) surface.<sup>35</sup> The adsorption energies of **7** and **8** are  $-2.50$  and



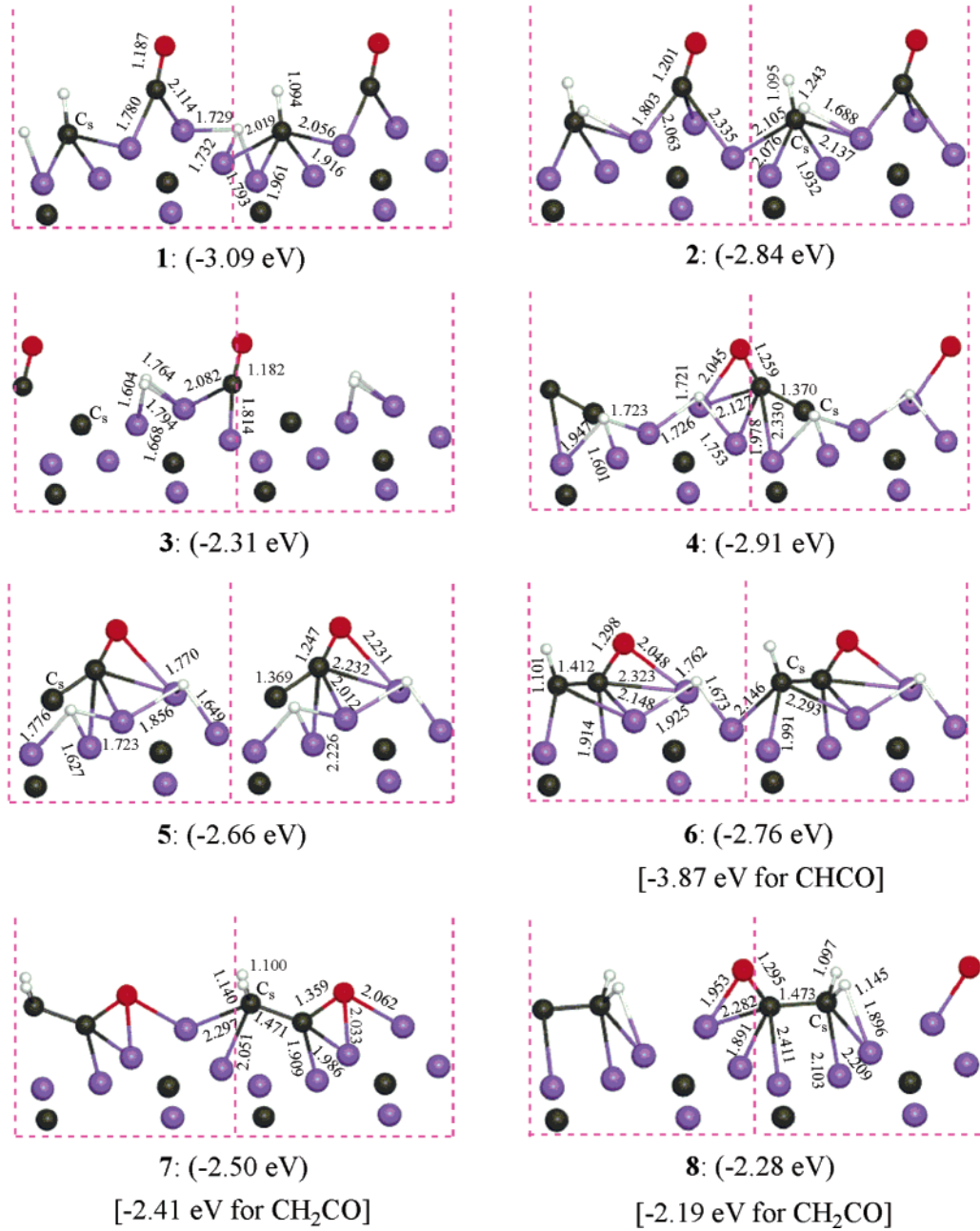


**Figure 2.** Coadsorption of H<sub>2</sub> at 1/6 ML and CO at 1/6 ML on Fe<sub>5</sub>C<sub>2</sub>(001) (Fe, purple; C, gray; O, red; H, white).  
**TABLE 2:** Computed Bond Lengths (*d*, Å) and Adsorption Energies (*E*<sub>ads</sub>, eV) for CO and H<sub>2</sub> Coadsorption on Fe<sub>5</sub>C<sub>2</sub>(001) with Coverages of 1/6 and 1/3 ML for H<sub>2</sub> and CO, Respectively (1/2 H<sub>2</sub>/CO)

	composition	<i>E</i> <sub>ads</sub>	<i>d</i> <sub>C–O</sub>		<i>d</i> <sub>C–Fe</sub>		<i>d</i> <sub>C–Cs</sub>		<i>d</i> <sub>O–Fe</sub>		<i>d</i> <sub>H–Fe</sub>		<i>d</i> <sub>H–Cs</sub>	<i>d</i> <sub>H–H</sub>
			a	b	a	b	a	b	a	b	a	b		
9	CO, C <sub>s</sub> CO, 2H	−4.05	1.177	1.244	1.914	2.011		1.365		2.075	1.632	1.653		
					1.940	2.109					1.710	1.740		
						2.236						1.773		
10	C <sub>s</sub> C <sub>2</sub> O <sub>2</sub> , 2H	−3.87	1.223	1.260	1.868	1.948	1.450	1.403	2.316	2.037	1.617	1.628		
					2.097	2.083					1.784	1.744		
						2.220					1.813	1.743		
11	CO, C <sub>s</sub> H <sub>2</sub> CO	−3.90 (−1.43) <sup>a</sup>	1.219	1.291	1.854	1.966		1.425		1.924	1.805		1.090	
					1.988	2.123						1.151		
					2.105	2.135								
12	CO, C <sub>s</sub> H <sub>2</sub> CO	−3.72 (−1.68) <sup>a</sup>	1.196	1.268	1.865	1.919		1.440		1.940	1.750		1.096	
					2.018	2.042						1.149		
					2.115									
13	CO, C <sub>s</sub> CO, H <sub>2</sub>	−3.47	1.236	1.252	2.156	1.883	1.352		2.284	2.212	1.633	1.641		0.864
					2.159	1.981								
					2.159	2.036								
						2.055								

<sup>a</sup> Using CH<sub>2</sub>CO as adsorbate.

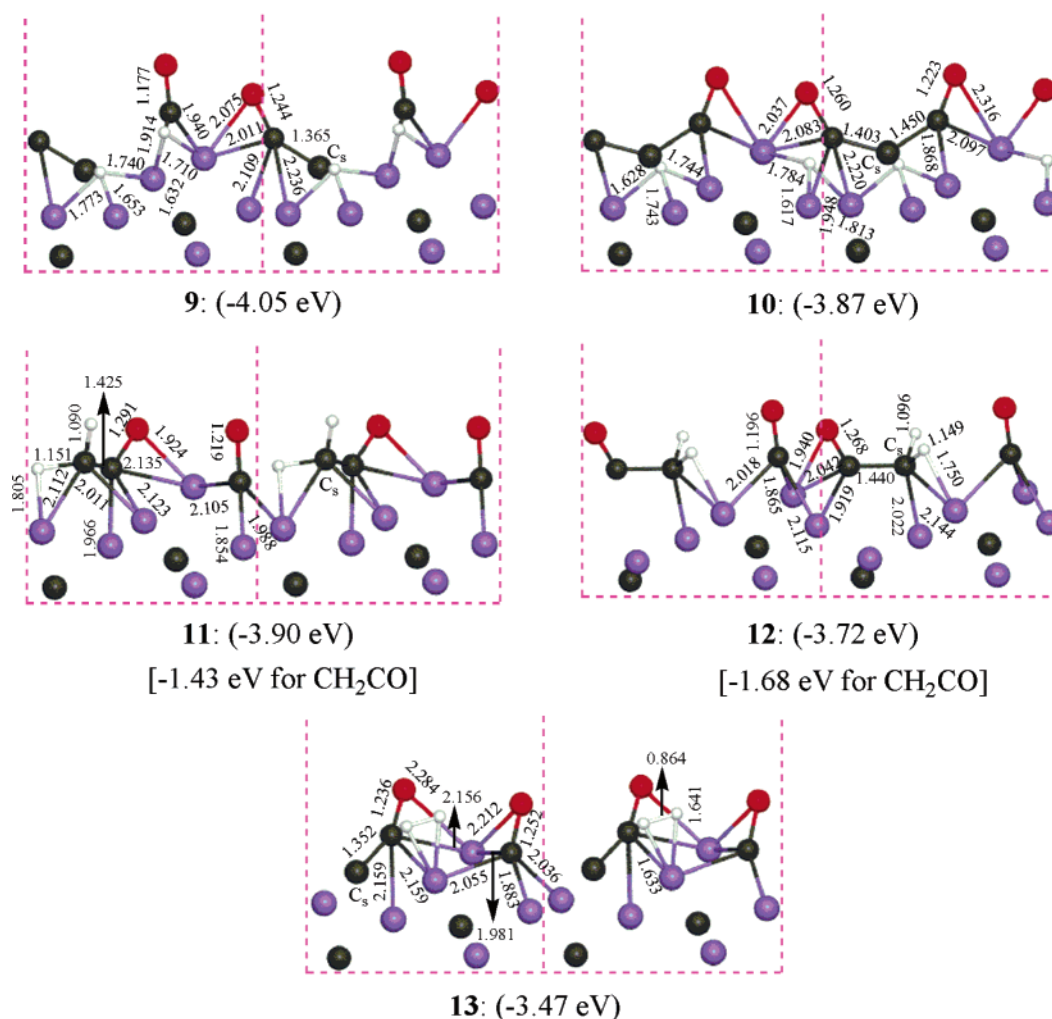


**Figure 3.** Coadsorption of H<sub>2</sub> at 1/6 ML and CO at 1/3 ML on Fe<sub>5</sub>C<sub>2</sub>(001) (Fe, purple; C, gray; O, red; H, white).

**TABLE 3: Computed Bond Lengths (*d*, Å) and Adsorption Energies (*E*<sub>ads</sub>, eV) for CO and H<sub>2</sub> Coadsorption on Fe<sub>5</sub>C<sub>2</sub>(001) with Coverages of 1/3 and 1/6 ML for H<sub>2</sub> and CO, Respectively (2/1 H<sub>2</sub>/CO)**

	composition	<i>E</i> <sub>ads</sub>	<i>d</i> <sub>C–O</sub>	<i>d</i> <sub>C–Fe</sub>	<i>d</i> <sub>C–C<sub>s</sub></sub>	<i>d</i> <sub>O–Fe</sub>	<i>d</i> <sub>H–Fe</sub>			<i>d</i> <sub>H–C<sub>s</sub></sub>
							a	b	c	
<b>14</b>	C <sub>3</sub> H <sub>2</sub> CO, 2H	–3.09 (–1.72) <sup>a</sup>	1.286	1.918	1.465	1.967	1.694	1.639	1.792	1.097
				2.238			1.733	1.703		1.158
				2.373			1.734	1.757		
<b>15</b>	C <sub>3</sub> H <sub>2</sub> CO, 2H	–3.02 (–1.65) <sup>a</sup>	1.308	1.975	1.482	2.034	1.623	1.681	1.690	1.094
				2.051			1.730	1.690		1.131
							1.821	1.803		
<b>16</b>	CO, 3H, C <sub>3</sub> H	–2.95	1.184	1.757			1.661	1.607	1.677	1.088
				2.114			1.663	1.679		
<b>17</b>	CO, 2H, C <sub>3</sub> H <sub>2</sub>	–2.67	1.196	1.844			1.606	1.648	1.645	1.088
				1.938			1.716	1.759		1.248

<sup>a</sup> Using CH<sub>2</sub>CO as adsorbate.

–2.28 eV when using CO and H<sub>2</sub> as adsorbates or –2.41 and –2.19 eV when using C<sub>3</sub>H<sub>2</sub>CO as the adsorbate, respectively.

We also investigated the adsorption patterns at a 1/2 H<sub>2</sub>/CO ratio on Fe<sub>5</sub>C<sub>2</sub>(001) (**9**–**13**). The coverages of H<sub>2</sub> and CO are 1/6 and 1/3 ML, respectively, and the computed bond parameters are given in Table 2 and Figure 3. In **9**, the adsorbed CO interacts with both surface iron and carbon, resulting in the formation of adsorbed ketylenide (C<sub>s</sub>CO) species. In contrast, the adsorbed H interacts only with surface iron. Similar to **9**, the adsorbed CO in **10** interacts with both surface iron and carbon, while the adsorbed H interacts only with iron. However, the most interesting point in **10** is the formation of the carbon suboxide (C<sub>3</sub>C<sub>2</sub>O<sub>2</sub>) pattern, and this shows the chain propagation,

which is essential for FTS. The adsorption energy in **9** is –4.05 eV, and that in **10** is –3.87 eV.

In **11** and **12**, the adsorbed CO and H interact with surface iron and carbon with the formation of surface adsorbed ketene (C<sub>3</sub>H<sub>2</sub>CO). In addition, one of the C<sub>s</sub>–H bonds in the C<sub>3</sub>H<sub>2</sub> unit interacts agostically with the neighbor iron atom by 1.151 and 1.149 Å for C<sub>s</sub>–H bonds and by 1.805 and 1.750 Å for Fe–H bonds, respectively. Along with the similar adsorbed surface species, both **11** and **12** have also close adsorption energies of –3.90 and –3.72 eV, respectively.

In **13**, however, there is H<sub>2</sub> (0.864 Å), C<sub>3</sub>CO, and CO. This indicates that H<sub>2</sub> dissociation is suppressed by the preadsorbed CO, in agreement with the experimental observation for the

**TABLE 4: Computed Bond Lengths ( $d$ , Å) and Adsorption Energies ( $E_{\text{ads}}$ , eV) for CO and H<sub>2</sub> Coadsorption on Fe<sub>5</sub>C<sub>2</sub>(110) with a Coverage of 1/6 ML for Both H<sub>2</sub> and CO (1/1 H<sub>2</sub>/CO)**

	composition	$E_{\text{ads}}$	$d_{\text{C-O}}$	$d_{\text{C-Fe}}$	$d_{\text{C-Cs}}$	$d_{\text{O-Fe}}$	$d_{\text{H-Fe}}$		$d_{\text{H-Cs}}$	$d_{\text{H-H}}$
							a	b		
18	CO, 2H	-3.07	1.173	1.784 2.312			1.640 1.730	1.613 1.738		
19	CO, 2H	-2.96	1.186	1.808 2.010			1.617 1.741	1.677 1.731		
20	CO, H, C <sub>s</sub> H	-2.45	1.205	1.857 2.055 2.081			1.712 1.743		1.104	
21	CO, H, C <sub>s</sub> H	-2.30	1.256	1.852 1.992 2.189 2.192		2.078	1.721 1.766		1.106	
22	C <sub>s</sub> CO, 2H	-2.86	1.270	1.994 2.066 2.242	1.417	2.070	1.760 1.725 1.838	1.687 1.764 1.842		
23	C <sub>s</sub> CO, 2H	-2.57	1.195	2.033	1.368		1.732 1.744 1.773	1.689 1.689		
24	C <sub>s</sub> H <sub>2</sub> CO	-2.14 (-2.43) <sup>a</sup>	1.338	2.042 2.173 2.279	1.459	1.882			1.094 1.107	
25	CO, H <sub>2</sub>	-2.62	1.253	1.861 1.947 2.244 2.207		2.105	1.627	1.647		0.880

<sup>a</sup> Using CH<sub>2</sub>CO as adsorbate.**TABLE 5: Computed Bond Lengths ( $d$ , Å) and Adsorption Energies ( $E_{\text{ads}}$ , eV) for CO and H<sub>2</sub> Coadsorption on Fe<sub>5</sub>C<sub>2</sub>(110) with Coverages of 1/6 and 1/3 ML for H<sub>2</sub> and CO, Respectively (1/2 H<sub>2</sub>/CO)**

	composition	$E_{\text{ads}}$	$d_{\text{C-O}}$		$d_{\text{C-Fe}}$		$d_{\text{C-Cs}}$		$d_{\text{O-Fe}}$		$d_{\text{H-Fe}}$		$d_{\text{H-Cs}}$	$d_{\text{H-H}}$
			a	b	a	b	a	b	a	b	a	b		
26	2CO, H, C <sub>s</sub> H	-5.03	1.169	1.182	1.747	1.798 2.124					1.565 1.829 1.977		1.105	
27	2CO, 2H	-4.70	1.162	1.189	1.760	1.882 1.980 2.337					1.638 1.735 1.917	1.660 1.799 1.846		
28	CO, C <sub>s</sub> CO, 2H	-4.33	1.273	1.185	1.928 2.227 2.233	1.854 1.993 2.269	1.424		2.045		1.589 1.739	1.718 1.739 1.805		
29	CO, C <sub>s</sub> CO, H <sub>2</sub>	-4.17	1.278	1.183	1.887 2.196 2.335	1.777 2.170	1.436		2.035		1.605 1.607		0.914	
30	CO, C <sub>s</sub> H <sub>2</sub> CO	-3.95 (-1.83) <sup>a</sup>	1.319	1.181	2.051 2.112 2.394	1.783 2.178	1.451		1.893				1.094 1.104	

<sup>a</sup> Using CH<sub>2</sub>CO as adsorbate.**TABLE 6: Computed Bond Lengths ( $d$ , Å) and Adsorption Energies ( $E_{\text{ads}}$ , eV) for CO and H<sub>2</sub> Coadsorption on Fe<sub>5</sub>C<sub>2</sub>(110) with Coverages of 1/3 and 1/6 ML for H<sub>2</sub> and CO, Respectively (2/1 H<sub>2</sub>/CO)**

	composition	$E_{\text{ads}}$	$d_{\text{C-O}}$	$d_{\text{C-Fe}}$	$d_{\text{C-Cs}}$	$d_{\text{O-Fe}}$	$d_{\text{H-Fe}}$				$d_{\text{H-Cs}}$	$d_{\text{H-H}}$
							a	b	c	d		
31	CO, 3H, C <sub>s</sub> H	-3.30	1.174	1.775 2.337			1.652 1.720	1.668 1.716	1.634 1.697		1.109	
32	C <sub>s</sub> CO, 4H	-3.05	1.194	1.915	1.425		1.621 1.714	1.633 1.772	1.652 1.742	1.640 1.721 1.804		
33	CO, H, C <sub>s</sub> H, H <sub>2</sub>	-3.30	1.190	1.825 1.978			1.673 1.766 1.868	1.580	1.607		1.111	0.941
34	C <sub>s</sub> H <sub>2</sub> CO, 2H	-3.24 (-2.09) <sup>a</sup>	1.314	1.991 2.058	1.427	1.910	1.726 1.732 1.798	1.691 1.762			1.090 1.100	

<sup>a</sup> Using CH<sub>2</sub>CO as adsorbate.

coadsorption of CO and H<sub>2</sub> on Fe(111),<sup>6</sup> Fe(100),<sup>7</sup> Pb(111), and Pb(100).<sup>10</sup> The adsorption energy of **13** is -3.47 eV, which is the weakest in the above five adsorption modes.

In addition, we are also interested in the adsorption patterns under the hydrogen-rich condition with a 2/1 H<sub>2</sub>/CO ratio (**14**–**17**). The coverages of H<sub>2</sub> and CO are 1/3 and 1/6 ML,

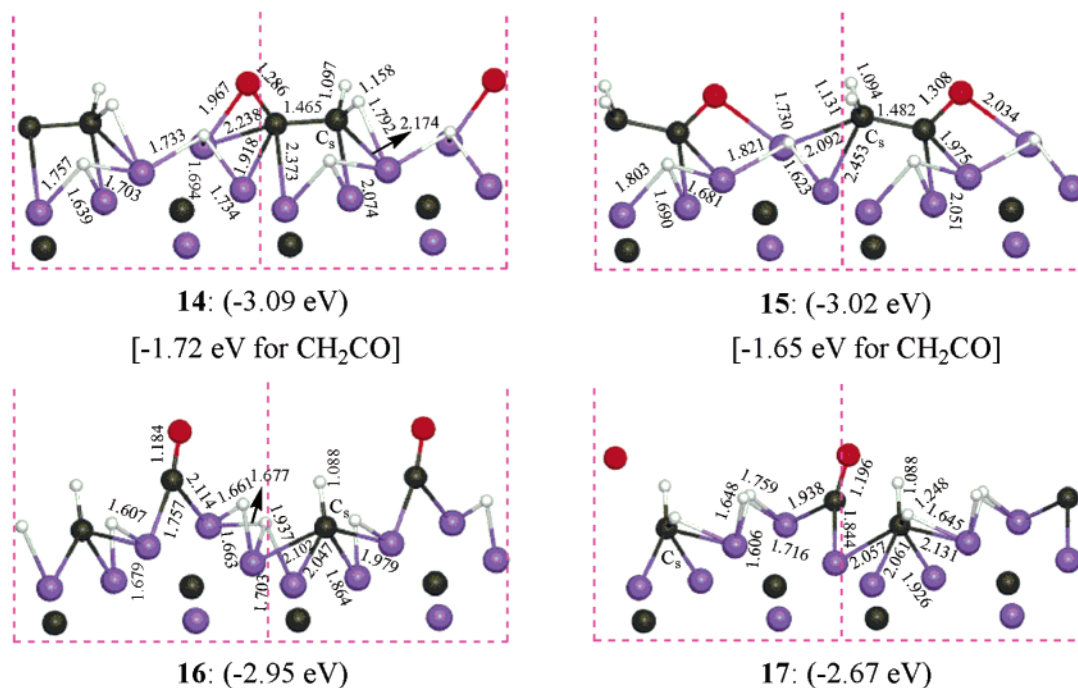


Figure 4. Coadsorption of H<sub>2</sub> at 1/3 ML and CO at 1/6 ML on Fe<sub>5</sub>C<sub>2</sub>(001) (Fe, purple; C, gray; O, red; H, white).

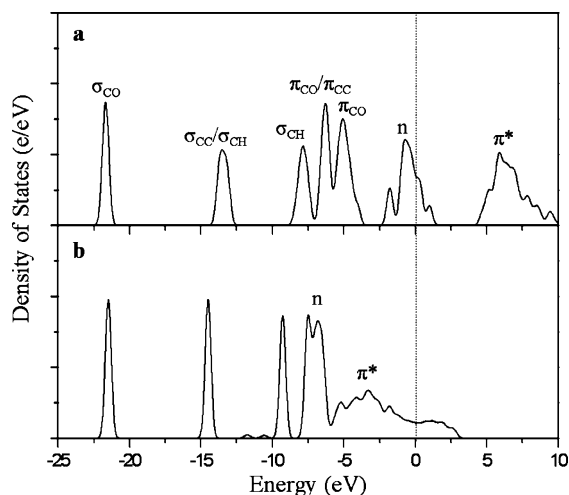


Figure 5. DOS of ketenyl CHCO (a) and adsorbed C<sub>5</sub>HCO in 6 (b).

respectively, and the bond parameters are given in Table 3 and Figure 4. In **14** and **15**, there is surface ketene (C<sub>5</sub>H<sub>2</sub>CO) formation and H species. The adsorption energies of **14** and **15** are very close (−3.09 and −3.02 eV). In **16** and **17**, however, the adsorbed CO interacts only with the surface iron, while the adsorbed H interacts with both surface iron and carbon. There is CO, H species, and C<sub>5</sub>H in **16**, while there is CO, H, and C<sub>5</sub>H<sub>2</sub> in **17**. The adsorption energies of **16** and **17** are −2.95 and −2.67 eV, respectively, and lower than those of **14** and **15**.

In addition, H<sub>2</sub> adsorption on oxygen atoms of adsorbed CO was also considered. H<sub>2</sub> was initially put on the top O atoms horizontally with a distance of 1.27 Å, but H<sub>2</sub> escapes from O atoms and becomes vertical to the surface and the distance of O and H is 2.708 Å. This indicates that it is not possible for direct O–H bond formation, in agreement with the observation in experiments.<sup>16</sup>

**3.1.2. Electronic Factor.** Since the electronic states of adsorbed hydrogen, CO, C<sub>5</sub>H, C<sub>5</sub>H<sub>2</sub>, and C<sub>5</sub>H<sub>3</sub> have been examined in our previous work,<sup>18,21</sup> we here intended to know the electronic features of the adsorbed ketenyl (C<sub>5</sub>HCO) in **6**, ketene (C<sub>5</sub>H<sub>2</sub>CO) in **7** and **8**, and carbon suboxide (C<sub>3</sub>C<sub>2</sub>O<sub>2</sub>) in

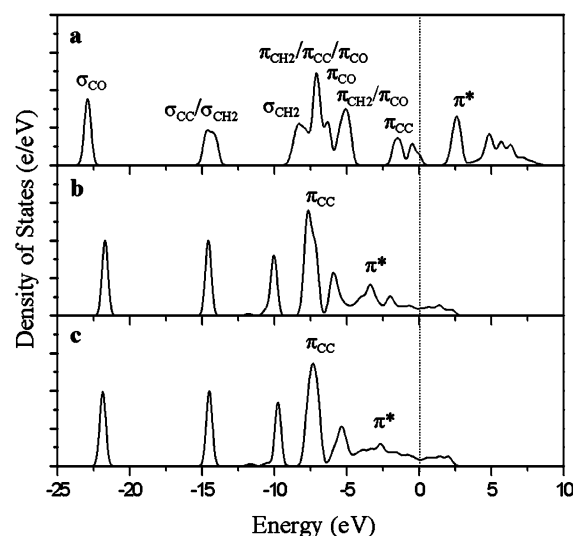


Figure 6. DOS of ketene CH<sub>2</sub>CO (a) and adsorbed C<sub>5</sub>H<sub>2</sub>CO in **7** (b) and **8** (c).

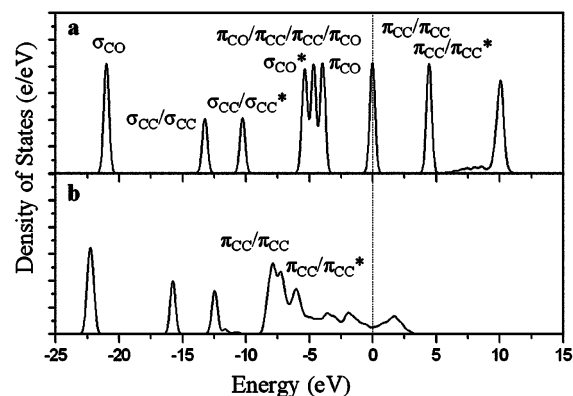
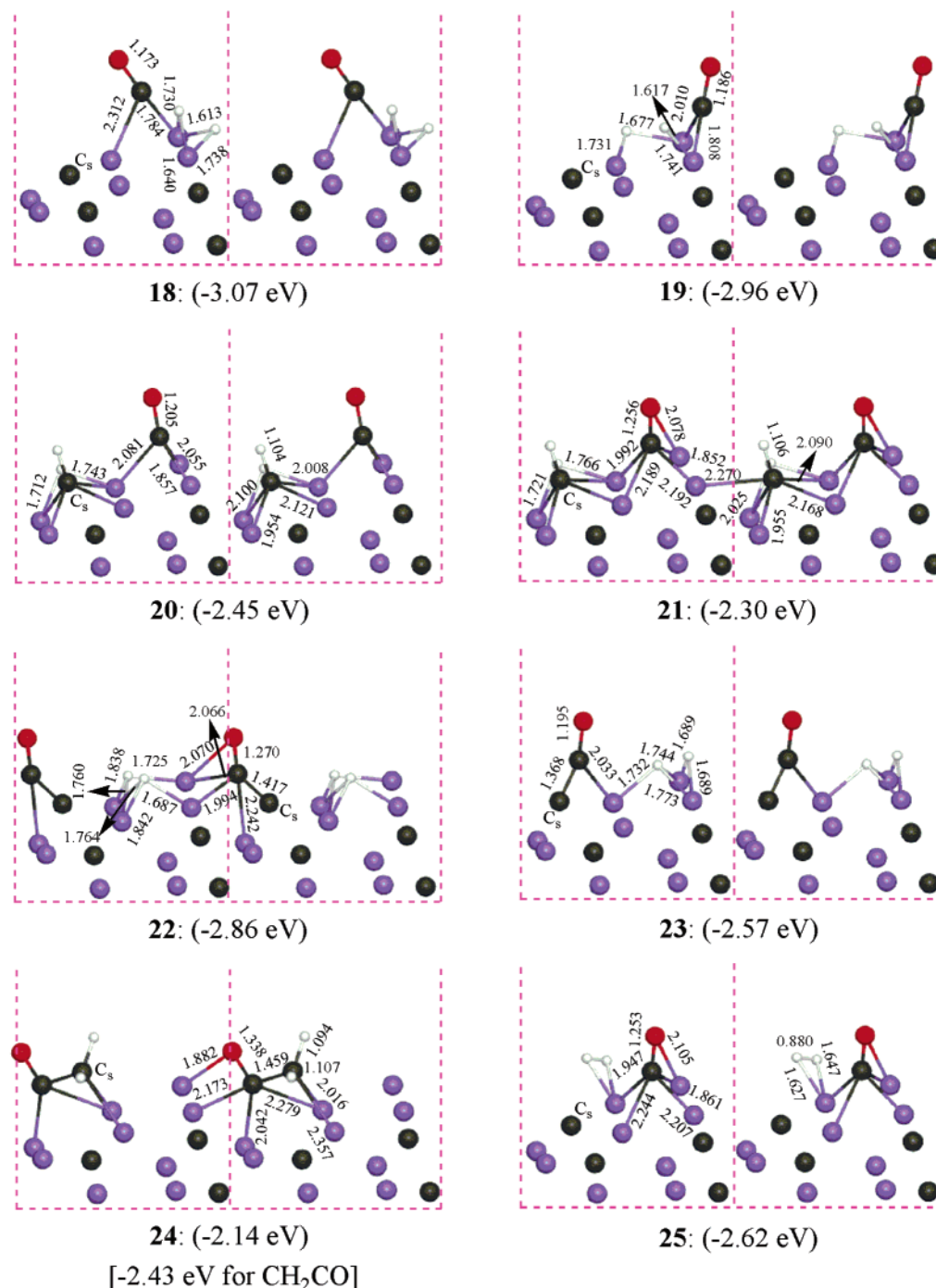


Figure 7. DOS of carbon suboxide C<sub>3</sub>O<sub>2</sub> (a) and adsorbed C<sub>5</sub>C<sub>2</sub>O<sub>2</sub> in **10** (b).

**10** for comparison. The density of states of free and adsorbed C<sub>5</sub>HCO are showed in Figure 5. In C<sub>5</sub>HCO (Figure 5a), the



**Figure 8.** Coadsorption of H<sub>2</sub> at 1/6 ML and CO at 1/6 ML on Fe<sub>5</sub>C<sub>2</sub>(110) (Fe, purple; C, gray; O, red; H, white).

frontier orbitals are the nonbonding (n) orbital at the range from -2.1 to 1.4 eV and the  $\pi^*$  orbital at about 5.7 eV.

After the adsorption, large shifts for both the n and  $\pi^*$  orbitals are found, and other bands have little changes in **6** (Figure 5b). The n band shifts downward to about -7.0 eV, while the  $\pi^*$  band shifts to the range from -5.0 to -4.1 eV. This explains the elongation of the C=C and C-O bond lengths from 1.256 to 1.412 Å and from 1.192 to 1.298 Å, respectively.

In **7** and **8**, surface C<sub>3</sub>H<sub>2</sub>CO is formed, and the density of states for free and adsorbed C<sub>3</sub>H<sub>2</sub>CO are showed in Figure 6. In C<sub>3</sub>H<sub>2</sub>CO (Figure 6a), the frontier orbitals are  $\pi_{CC}$  lying from -1.7 to 0.3 eV and the  $\pi^*$  orbital at about 2.6 eV. After the adsorption (Figure 6b and c), as expected, large shifts for  $\pi_{CC}$  and the  $\pi^*$  orbital band are found. For example,  $\pi_{CC}$  shifts downward to about -7.6 and -7.3 eV in **7** and **8**, while  $\pi^*$

shifts downward strongly to the range from -4.0 to -3.5 and -4.0 to -3.6 eV in **7** and **8**, respectively.

The surface carbon suboxide (C<sub>s</sub>C<sub>2</sub>O<sub>2</sub>) is formed in **10**. The density of states of free and adsorbed C<sub>3</sub>O<sub>2</sub> are showed in Figure 7. In free C<sub>3</sub>O<sub>2</sub>, the frontier orbitals are  $\pi_{CC}/\pi_{CC}$  and  $\pi_{CC}/\pi_{CC}^*$ , and they lie at about 0.0 and 4.4 eV, respectively. After adsorption (Figure 7b), they shift downward strongly, for example,  $\pi_{CC}/\pi_{CC}$  to -7.6 eV and  $\pi_{CC}/\pi_{CC}^*$  to -5.4 eV, respectively.

**3.2. Coadsorption of CO and H<sub>2</sub> on Fe<sub>5</sub>C<sub>2</sub>(110).** **3.2.1. Structure and Energy.** For the bare Fe<sub>5</sub>C<sub>2</sub>(110) surface with a 1/1 H<sub>2</sub>/CO ratio, the coverages of H<sub>2</sub> and CO are both 1/6 ML. Eight optimized forms (**18**–**25**) are shown in Figure 8, and the computed adsorption energies and structural parameters are listed in Table 4. Both **18** and **19** consist of CO and H species,



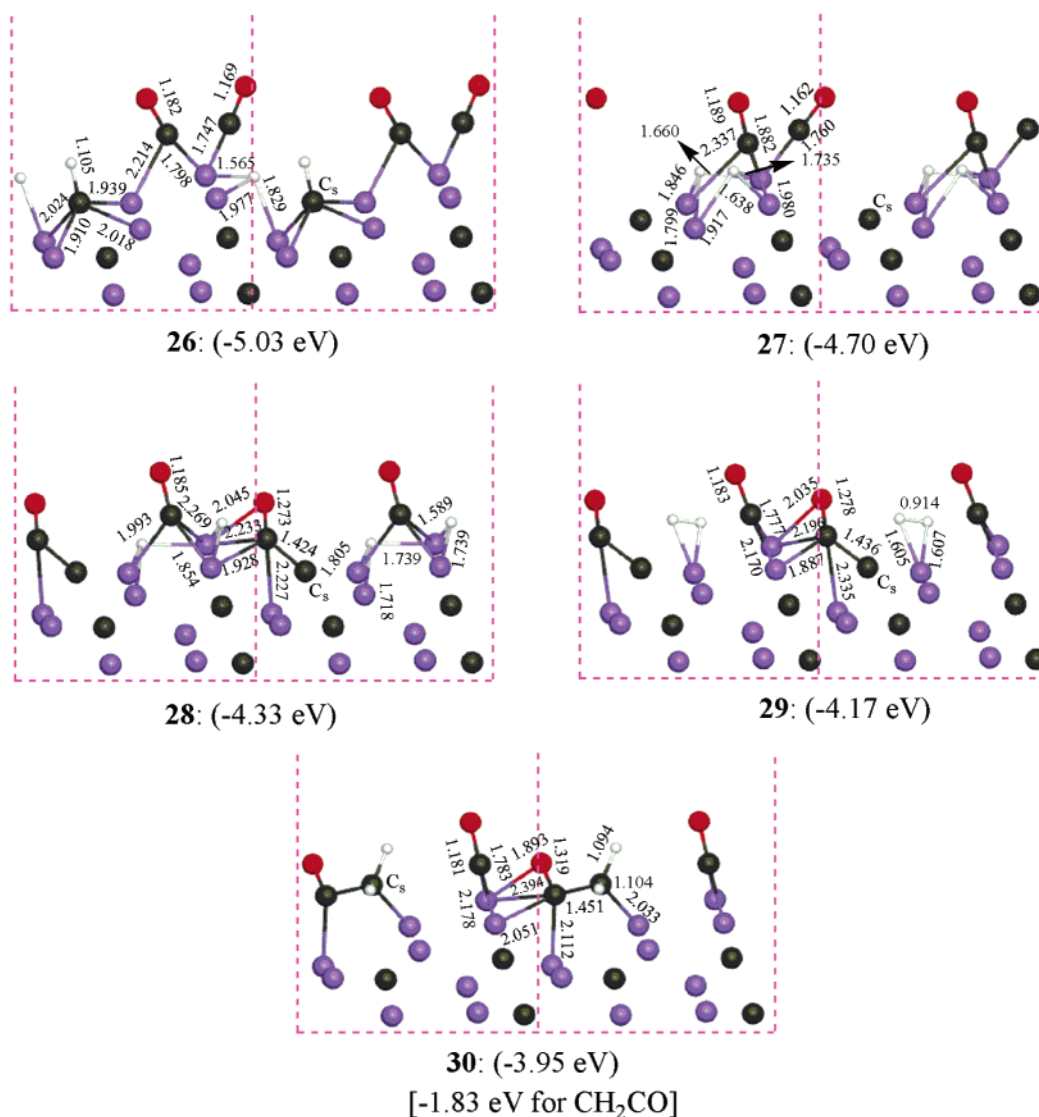


**Figure 9.** Coadsorption of H<sub>2</sub> at 1/6 ML and CO at 1/3 ML on Fe<sub>5</sub>C<sub>2</sub>(110) (Fe, purple; C, gray; O, red; H, white).

with adsorption energies of  $-3.07$  and  $-2.96$  eV, respectively. Species **20** and **21** are composed of CO, H, and C<sub>5</sub>H. The adsorption energies of **20** and **21** are  $-2.45$  and  $-2.30$  eV, respectively. In both **22** and **23**, ketenylidene (C<sub>5</sub>CO) is formed. The adsorption energies of **22** and **23** are  $-2.86$  and  $-2.57$  eV, respectively.

In **24**, both adsorbed CO and H interact with surface iron and carbon with the formation of ketene (C<sub>5</sub>H<sub>2</sub>CO). The adsorption energy of **24** is  $-2.14$  eV. If using C<sub>5</sub>H<sub>2</sub>CO as adsorbate, the adsorption energy is  $-2.43$  eV, which is similar to that on Fe<sub>5</sub>C<sub>2</sub>(001). **25** consists of CO and one activated H<sub>2</sub> (H–H,  $0.880$  Å), and the adsorption energy is  $-2.62$  eV.

For a 1/2 H<sub>2</sub>/CO ratio, the coverages 1/6 ML for H<sub>2</sub> and 1/3 ML for CO are considered. There are five modes (**26**–**30**), and the computed parameters are shown in Figure 9 and Table 5. **26** consists of CO, H, and C<sub>5</sub>H, while **27** consists of CO and H species. The adsorption energies of **26** and **27** are  $-5.03$  and  $-4.70$ , respectively.

In both **28** and **29**, there is ketenylidene (C<sub>5</sub>CO) formation on the surface. The adsorbed H<sub>2</sub> is dissociated in **28**, but H<sub>2</sub> is only activated with a bond length of  $0.914$  Å in **29**. The adsorption energies of **28** and **29** are  $-4.33$  and  $-4.17$  eV, respectively. In **30**, surface ketene (C<sub>5</sub>H<sub>2</sub>CO) is formed, and the adsorption energy of  $-3.95$  eV is the lowest among **26**–

**30**. Using C<sub>5</sub>H<sub>2</sub>CO as adsorbate, the adsorption energy is  $-1.83$  eV, which is much lower than that at a 1/1 H<sub>2</sub>/CO ratio ( $-2.43$  eV), indicating the repulsion between CO and C<sub>5</sub>H<sub>2</sub>CO.

For a 2/1 H<sub>2</sub>/CO ratio, coverages of 1/3 ML for H<sub>2</sub> and 1/6 ML for CO are considered. There are four adsorption patterns (**31**–**34**) given in Table 6 and Figure 10. In **31**, there is CO, H, and C<sub>5</sub>H. The adsorption energy of **31** ( $-3.30$  eV) is the highest. In **32**, there are ketenylidene (C<sub>5</sub>CO) and H species. The adsorption energy of **32** ( $-3.05$  eV) is the lowest. In **33**, there is CO, H species, C<sub>5</sub>H, and H<sub>2</sub> ( $0.941$  Å). The adsorption energy of **33** is the same as **31**. In **34**, there are adsorbed C<sub>5</sub>H<sub>2</sub>CO and H species with an adsorption energy of  $-3.24$  eV. Taking C<sub>5</sub>H<sub>2</sub>CO as adsorbate, the adsorption energy is  $-2.09$  eV.

**3.2.2. Electronic Factor.** The ketene (C<sub>5</sub>H<sub>2</sub>CO) is formed in **24** on (110). The density of states of free C<sub>5</sub>H<sub>2</sub>CO and adsorbed one are showed in Figure 10. After adsorption (Figure 11b), as expected, large shifts for the  $\pi_{CC}$  and  $\pi^*$  orbital bands are found (other bands have a little shift). The  $\pi_{CC}$  band shifts downward to about  $-7.9$  eV in **24**, while the  $\pi^*$  band shifts downward strongly to the range from  $-4.0$  to  $-3.5$  eV. These changes are comparable to those in **7** and **8** (Figure 6).

**3.3. Coadsorption of CO and H<sub>2</sub> on Fe<sub>5</sub>C<sub>2</sub>(100).** Since the bare Fe<sub>5</sub>C<sub>2</sub>(100) monolayer is only composed of iron atoms, the adsorption patterns are less complicated as compared to those

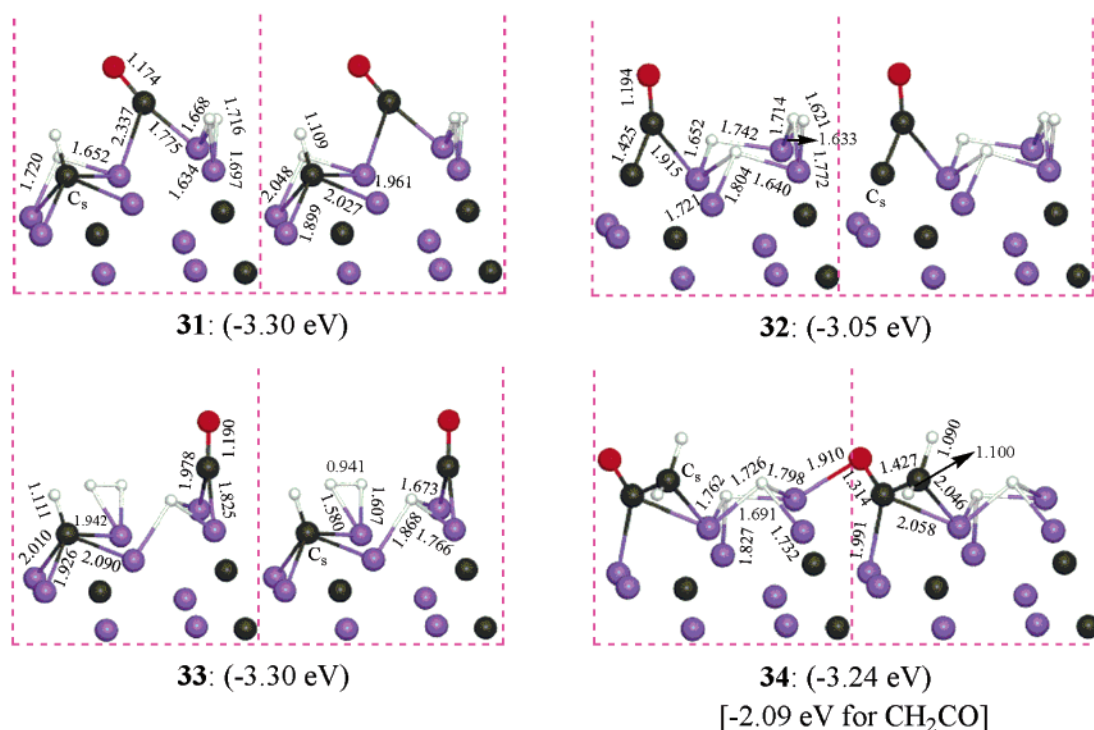


Figure 10. Coadsorption of H<sub>2</sub> at 1/3 ML and CO at 1/6 ML on Fe<sub>5</sub>C<sub>2</sub>(110) (Fe, purple; C, gray; O, red; H, white).

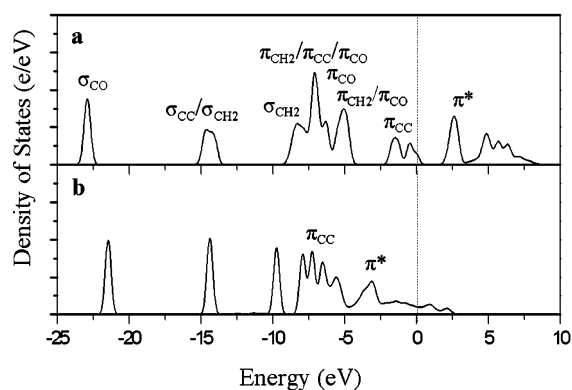


Figure 11. DOS of ketene C<sub>3</sub>H<sub>2</sub>CO (a) and adsorbed C<sub>3</sub>H<sub>2</sub>CO in 24 (b).

on (001) and (110). For a 1/1 H<sub>2</sub>/CO ratio with a 1/4 ML coverage for both H<sub>2</sub> and CO, there are 10 forms (**35–44**), and the calculated parameters are given in Table 7 and Figure 12.

Species **35–38** are composed of 2-fold CO and H species, and the adsorption energies are -3.30, -3.30, -3.39, and -3.30 eV, respectively. Species **39–42** are composed of top-CO and H, and the adsorption energies are -3.36, -3.34, -3.41, and -3.41 eV, respectively, which are comparable to those of **35–38**. In **43** and **44**, there are top-CO and activated H<sub>2</sub>, and the adsorption energies (-2.73 and -2.72 eV) are lower than those of **35–42**. This indicates that dissociated H is more favored (100) than activated molecular H<sub>2</sub>.

For a 1/2 H<sub>2</sub>/CO ratio with coverages of 1/4 ML for H<sub>2</sub> and 1/2 ML for CO, there are three modes (**45–47**), and the computed parameters are shown in Table 8 and Figure 13. **45** consists of 2-fold CO, while **46** and **47** consist of top-CO. The adsorption energies of **46** (-3.36 eV) and **47** (-3.31 eV) are lower than that of **45** (-4.93 eV).

For a 2/1 H<sub>2</sub>/CO ratio with coverages of 1/2 ML for H<sub>2</sub> and 1/4 ML for CO, there are six forms (**48–53**), and the optimized parameters are given in Table 9 and Figure 14. In **48** and **49**, CO is adsorbed at 2-fold sites, and H<sub>2</sub> is all dissociated. The

TABLE 7: Computed Bond Lengths (*d*, Å) and Adsorption Energies (*E*<sub>ads</sub>, eV) for CO and H<sub>2</sub> Coadsorption on Fe<sub>5</sub>C<sub>2</sub>(100) with a Coverage of 1/4 ML for Both H<sub>2</sub> and CO (1/1 H<sub>2</sub>/CO)

	composition	<i>E</i> <sub>ads</sub>	<i>d</i> <sub>C–O</sub>	<i>d</i> <sub>C–Fe</sub>	<i>d</i> <sub>H–Fe</sub>		<i>d</i> <sub>H–H</sub>
					a	b	
35	CO, 2H	-3.30	1.186	1.802	1.599	1.711	
					2.178	1.726	
36	CO, 2H	-3.30	1.185	1.806	1.591	1.716	
					2.139	1.717	
37	CO, 2H	-3.39	1.183	1.811	1.600	1.628	
					2.095	1.777	
38	CO, 2H	-3.30	1.181	1.862	1.654	1.667	
					2.050	1.727	
39	CO, 2H	-3.36	1.168	1.760	1.685	1.647	
					1.755	1.778	
40	CO, 2H	-3.34	1.170	1.771	1.777	1.863	
					1.682	1.655	
41	CO, 2H	-3.41	1.168	1.752	1.764	1.801	
					1.774	1.841	
42	CO, 2H	-3.41	1.169	1.755	1.606	1.676	
					1.811	1.765	
43	CO, H <sub>2</sub>	-2.73	1.167	1.790	1.814	1.781	
					1.673	1.608	
44	CO, H <sub>2</sub>	-2.72	1.167	1.796	1.764	1.807	
					1.791	1.833	

adsorption energies of **48** and **49** are close (-3.68 and -3.65 eV, respectively). In **50–53**, CO is adsorbed at top sites. H<sub>2</sub> is all dissociated in **50** and **51**, while H<sub>2</sub> is not all dissociated in **52** and **53**. The adsorption energies of **50–53** are -3.64, -3.62, -3.55, and -3.53 eV, respectively.

#### 4. Discussion

On the Fe<sub>5</sub>C<sub>2</sub>(001) surface at 1/6 ML under coadsorption with a 1/1 H<sub>2</sub>/CO ratio, the most stable surface species are 2-fold

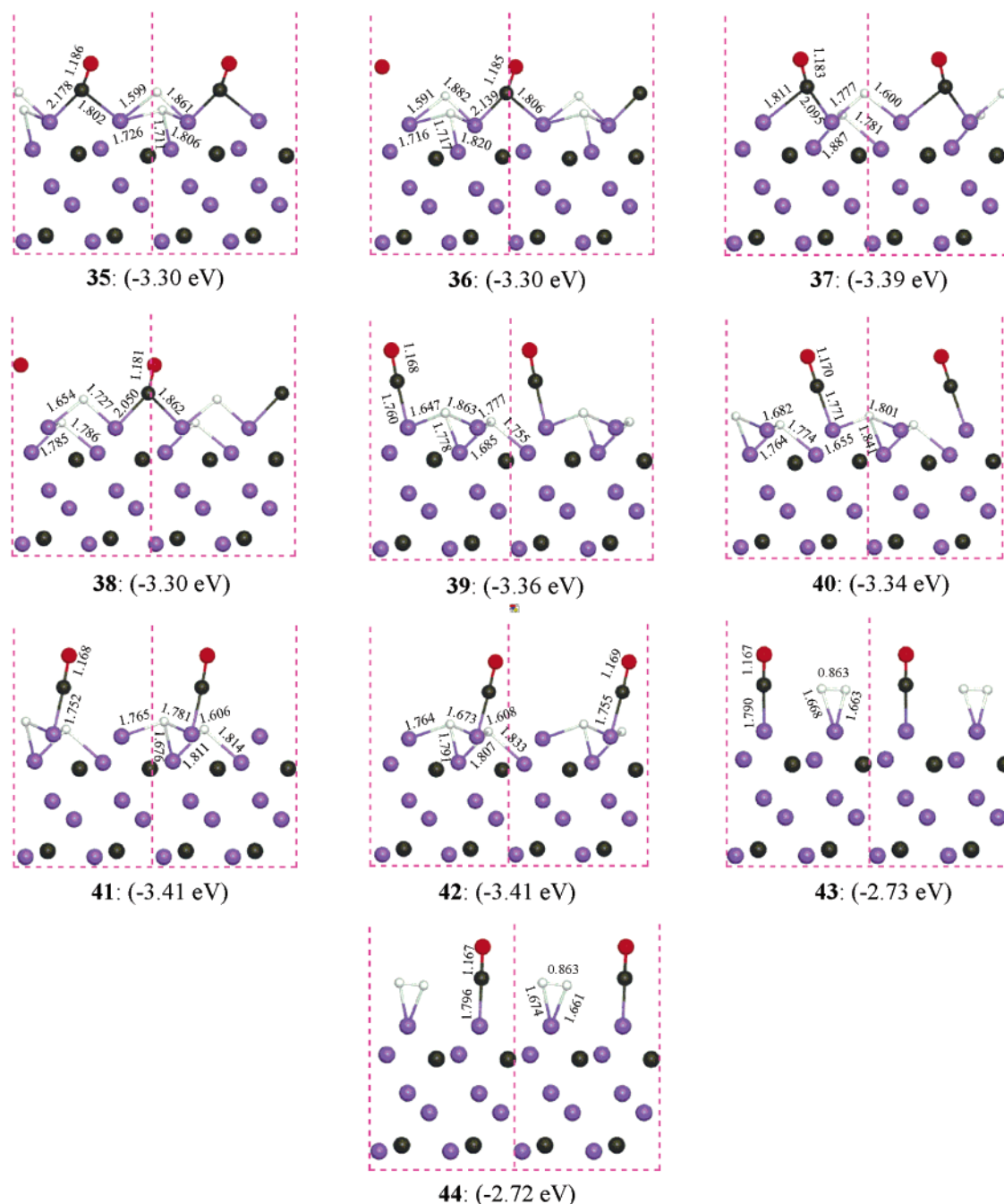


**Figure 12.** Coadsorption of H<sub>2</sub> at 1/4 ML and CO at 1/4 ML on Fe<sub>5</sub>C<sub>2</sub>(100) (Fe, purple; C, gray; O, red; H, white).

**TABLE 8: Computed Bond Lengths (*d*, Å) and Adsorption Energies (*E*<sub>ads</sub>, eV) for CO and H<sub>2</sub> Coadsorption on Fe<sub>5</sub>C<sub>2</sub>(100) with Coverages of 1/4 and 1/2 ML for H<sub>2</sub> and CO, Respectively (1/2 H<sub>2</sub>/CO)**

composition	<i>E</i> <sub>ads</sub>	<i>d</i> <sub>C–O</sub>		<i>d</i> <sub>C–Fe</sub>		<i>d</i> <sub>H–Fe</sub>	
		a	b	a	b	a	b
45	-4.93	1.173	1.180	1.842	1.902	1.601	1.663
				2.105	1.960	1.705	1.738
							1.789
46	-3.36	1.160	1.161	1.803	1.772	1.683	1.595
						1.735	1.772
						1.775	1.850
47	-3.31	1.161	1.162	1.786	1.766	1.578	1.677
						1.750	1.686
							1.860

CO, 4-fold C<sub>s</sub>H, and 3-fold H species, while the surface C<sub>s</sub>H<sub>2</sub> is less stable and may dissociate into C<sub>s</sub>H and H. This is the

same as found for hydrogen adsorption, in which 3-fold H and surface C<sub>s</sub>H are the most stable species, and C<sub>s</sub>H<sub>2</sub> is less stable.<sup>18</sup> In contrast with H<sub>2</sub>/CO coadsorption, the surface species in CO adsorption<sup>21</sup> (3-fold CO and the formed surface C<sub>s</sub>CO from CO interacting with surface iron and carbon in different forms) are close in energy. Moreover, H<sub>2</sub>/CO coadsorption shows the possibility for the formation of surface species including C<sub>s</sub>CO, C<sub>s</sub>HCO, and C<sub>s</sub>H<sub>2</sub>CO, and this is essentially related to the chain elongation in FTS.

C<sub>s</sub>H is very stable and is a potential species for the formation of C<sub>s</sub>H<sub>2</sub> and C<sub>s</sub>H<sub>3</sub>, which are also important for FTS. Ketenylidene (C<sub>s</sub>CO), ketenyl (C<sub>s</sub>HCO), and ketene (C<sub>s</sub>H<sub>2</sub>CO) are formed by CO addition to surface carbon atoms. An amount of surface carbon atoms exists on active Fe<sub>2</sub>C catalysts<sup>36</sup> and can take part in the chain coupling reaction.<sup>37</sup> Moreover, ketenylidene and ketene have been observed in metal ketenylidene and carbonyl cluster<sup>38</sup> [Fe<sub>3</sub>(CO)<sub>9</sub>(CCO)]<sup>2-</sup> and on Fe surfaces

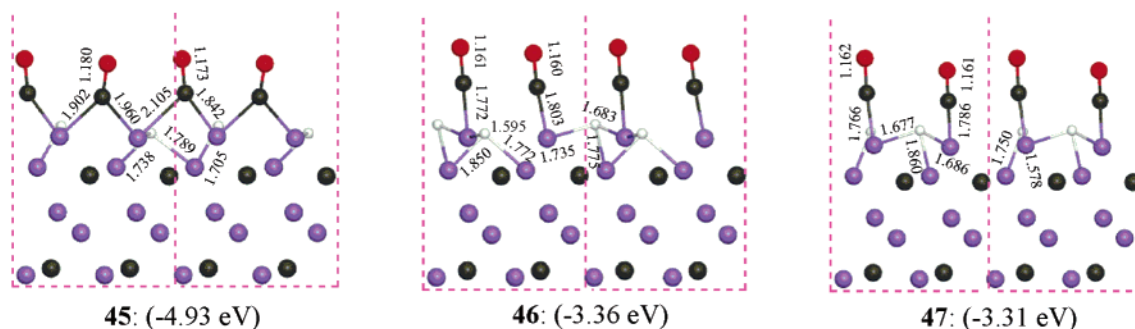


Figure 13. Coadsorption of H<sub>2</sub> at 1/4 ML and CO at 1/2 ML on Fe<sub>5</sub>C<sub>2</sub>(100) (Fe, purple; C, gray; O, red; H, white).

TABLE 9: Computed Bond Lengths ( $d$ , Å) and Adsorption Energies ( $E_{\text{ads}}$ , eV) for CO and H<sub>2</sub> Coadsorption on Fe<sub>5</sub>C<sub>2</sub>(100) with Coverages of 1/2 and 1/4 ML for H<sub>2</sub> and CO, Respectively (2/1 H<sub>2</sub>/CO)

composition	$E_{\text{ads}}$	$d_{\text{C-O}}$	$d_{\text{C-Fe}}$	$d_{\text{H-Fe}}$				$d_{\text{H-H}}$
				a	b	c	d	
48 CO, 4H	-3.68	1.175	1.786	1.661	1.606	1.619	1.551	
				2.196	1.680	1.776	1.772	
49 CO, 4H	-3.65	1.176	1.776	1.587	1.663	1.571	1.665	
				2.219	1.842	1.738	1.813	
50 CO, 4H	-3.64	1.165	1.751	1.627	1.577	1.660	1.657	
				1.761	1.711	1.667	1.726	
51 CO, 4H	-3.62	1.163	1.758	1.660	1.589	1.648	1.647	
				1.740	1.697	1.710	1.698	
52 CO, 2H, H <sub>2</sub>	-3.55	1.170	1.756	1.674	1.613	1.635	1.637	0.851
				1.766	1.769	1.771	1.843	
53 CO, 2H, H <sub>2</sub>	-3.53	1.171	1.759	1.618	1.685	1.642	1.645	0.847
				1.747	1.751	1.844	1.776	

in experiments.<sup>20</sup> Therefore, it is possible for ketenylidene, ketenyl, and ketene formation on Fe<sub>5</sub>C<sub>2</sub>(001) and (110). In addition, Liu et al.'s theoretical study indicated that the reaction of C + CH is the favored pathway in the C/C coupling reactions on the Ru-step surfaces.<sup>39</sup> Ketene with C=C and C=O bonds is the key structure for forming hydrocarbons and ethanol.<sup>40</sup> Therefore, the reactions of ketene hydrogenation and its C—O bond cleavage are also an initial and important step of FTS. The study of the thermodynamic and kinetic properties of ketene on a catalyst surface with adsorbed CO/H<sub>2</sub> are also very interesting and exciting and will be investigated further.

With the increased CO coverage under coadsorption on Fe<sub>5</sub>C<sub>2</sub>(001) and a 1/2 H<sub>2</sub>/CO ratio, the surfaces C<sub>5</sub>CO, C<sub>5</sub>H<sub>2</sub>CO, and carbon suboxide (C<sub>5</sub>C<sub>2</sub>O<sub>2</sub>) possibly coexist. This is in agreement with that of CO adsorption,<sup>21</sup> where the adsorbed CO interacts not only with surface iron but also with carbon, resulting in the formation of C<sub>2</sub> and C<sub>3</sub> units on the surface.

The surface carbon suboxide (C<sub>5</sub>C<sub>2</sub>O<sub>2</sub>) on Fe<sub>5</sub>C<sub>2</sub>(001) is very interesting but has not been observed experimentally over iron catalysts. Although carbon suboxide is stable thermodynamically, its kinetic property for the reaction of C<sub>5</sub>C<sub>2</sub>O<sub>2</sub> hydrogenation as well as C=C and C=O bond cleavage is also very important. For example, the long C—O bond of the carbon suboxide is likely easy to be broken, resulting in the formation of the hydrocarbons and oxygenate at C<sub>3</sub> in FTS. In addition, CO can add to the middle carbon atom and leads to the formation of the branch chain products. Therefore, further studies of the thermodynamic and kinetic properties of the species formed by CO insertion are required to understand the genesis of the FTS reaction mechanism.

With the increased H coverage under coadsorption and a 2/1 H<sub>2</sub>/CO ratio on Fe<sub>5</sub>C<sub>2</sub>(001), the surface H, C<sub>5</sub>H, and C<sub>5</sub>H<sub>2</sub>CO are the most stable species. Similarly, for pure hydrogen adsorption at the same coverage with coadsorption on Fe<sub>5</sub>C<sub>2</sub>(001), the most stable surface species are CH, activated H<sub>2</sub>, and H species.<sup>18</sup>

On the Fe<sub>5</sub>C<sub>2</sub>(110) surface at 1/6 ML with a 1/1 H<sub>2</sub>/CO ratio, the most stable surface species are 2-fold CO and two 2-fold H species. Similar to hydrogen adsorption,<sup>18</sup> the most stable species is one 2-fold and one 3-fold H species. In contrast to CO adsorption,<sup>21</sup> the surface species of H<sub>2</sub>/CO coadsorption (2-fold CO and the formed surface C<sub>5</sub>CO from CO interacting with surface iron and carbon) can also coexist due to their similar adsorption energies. Similar to (001), CH<sub>2</sub>CO is also formed by H<sub>2</sub>/CO coadsorption.

With increased CO coverage (1/2 H<sub>2</sub>/CO) under coadsorption, surface species, CO, C<sub>5</sub>H, and H, can coexist, as they are energetically stable. The order of adsorption energy of the surface species and their geometries is in agreement with that of CO adsorption at the same coverage. With the increased H coverage (2/1 H<sub>2</sub>/CO) under coadsorption along with surface H, C<sub>5</sub>H and C<sub>5</sub>H<sub>2</sub>CO are the most stable surface species. In contrast, the most stable surface species for hydrogen adsorption consist of C<sub>5</sub>H, 2-fold and 3-fold H species.

The adsorption energies indicate that the stability of the Fe<sub>5</sub>C<sub>2</sub>(001) and (110) surfaces with surface ketene species is greater when the surface concentration of H<sub>2</sub> is larger than that of CO (i.e., for the 2/1 H<sub>2</sub>/CO ratio). At the other hydrogen coverage (i.e., for the 1/1 and 1/2 H<sub>2</sub>/CO ratios), surface ketene species become less stable. This indicates ketene formation is favored under the hydrogen-rich condition. The reason is that ketene (C<sub>5</sub>H<sub>2</sub>CO) is formed by C<sub>5</sub>CO hydrogenation. On (001) and (110), the adsorption energy of the species consisting of C<sub>5</sub>CO and 2H is higher than that of ketene for the 1/1 and 1/2 H<sub>2</sub>/CO ratios, while the adsorption energy of the species consisting of C<sub>5</sub>CO and 4H coexisting is lower than that of C<sub>5</sub>H<sub>2</sub>CO and 2H coexisting for the 2/1 H<sub>2</sub>/CO ratio. For the formal reaction of ketene formation, C<sub>5</sub>CO + H<sub>2</sub> → C<sub>5</sub>H<sub>2</sub>CO, at high H<sub>2</sub> coverage (high H<sub>2</sub> surface concentration), the reaction is favored and results in a high concentration of C<sub>5</sub>H<sub>2</sub>CO; in contrast, at low H<sub>2</sub> coverage, the back reaction is favored and results in a high concentration of C<sub>5</sub>CO.

Different from Fe<sub>5</sub>C<sub>2</sub>(001) and (110), the top layer of Fe<sub>5</sub>C<sub>2</sub>(100) consists originally only of iron atoms and therefore is metallic in character. On Fe<sub>5</sub>C<sub>2</sub>(100) at 1/4 ML under coadsorption with a 1/1 H<sub>2</sub>/CO ratio, the most stable surface species are top- and 2-fold CO as well as 2-fold and 3-fold H species. This is inconsistent with CO adsorption,<sup>21</sup> where the top- and 3-fold CO are close in energy. With increased CO coverage (1/2 H<sub>2</sub>/CO), the possible surface species are 2-fold CO and 2-fold and 3-fold H. The change of CO configurations



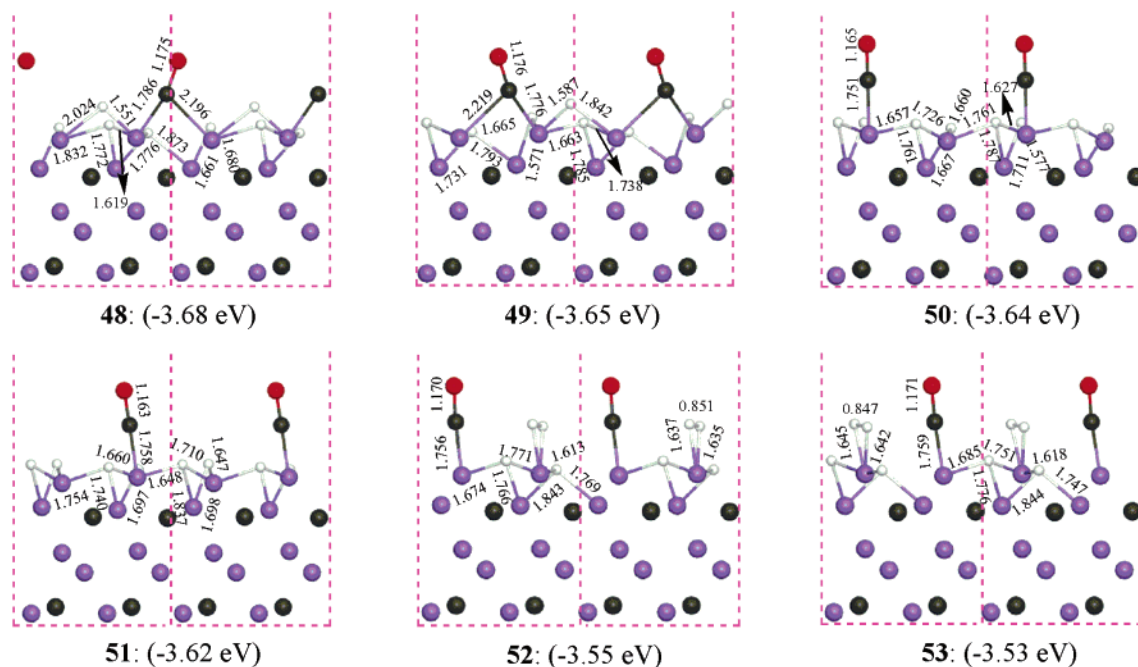


**Figure 14.** Coadsorption of  $\text{H}_2$  at 1/2 ML and CO at 1/4 ML on  $\text{Fe}_5\text{C}_2(100)$  (Fe, purple; C, gray; O, red; H, white).

is similar with the CO adsorption on  $\text{Fe}(111)$ .<sup>41</sup> In only CO adsorption at 1/2 ML, CO is favored to adsorb at the 3-fold site. With the increased H coverage (2/1  $\text{H}_2/\text{CO}$ ), the possible surface species are 2-fold and 3-fold H, in agreement with the case for  $\text{H}_2$  adsorption<sup>18</sup> at the same coverage. Due to the composition of CO and H species on (100), therefore, cleavage of C–O bonds on (100) is the first important step of FTS.

For all species on the three surfaces, CO is not dissociated directly. Thus, the reaction of C–O bond cleavage is also an important step followed by  $\text{C}_x\text{H}_y$  formation in the FTS. Since CO is favored to absorb at 2-fold, 3-fold, and 4-fold sites on  $\text{Fe}_5\text{C}_2(001)$ , at 2-fold and 4-fold sites on (110), and at 2-fold sites on (100), the C–O distances lie in the wide range from 1.160 to 1.359 Å. It is possible for the CO dissociation mechanism to be direct and indirect for these diverse adsorbed sites on these surfaces. The indirect dissociation is the formate mechanism, in which molecular adsorbed CO yields the two intermediates  $\text{M}-\text{CHO}$  and  $\text{M}-\text{COH}$  (M, metal) upon the addition of a hydrogen atom and then  $\text{M}-\text{CHOH}$  and  $\text{M}-\text{CH}_2\text{OH}$  after further hydrogenation. During this process, the hydroxyl O–H rather than C–O vibrations were observed on silica-supported nickel<sup>42</sup> and silica-supported iron,<sup>43</sup> and formyl CHO and formate were detected by vibrational frequency analysis on  $\text{Ni}(111)$ .<sup>44</sup>

Along with the investigation into the individual adsorption of CO and  $\text{H}_2$ , our current study about the CO/ $\text{H}_2$  coadsorption on these  $\text{Fe}_5\text{C}_2$  surfaces provides some new insights into the mechanism of FTS. However, it is still far away from the full understanding of the FTS mechanism, and studies about the thermodynamic and kinetic processes on the surfaces will be continued.

## 5. Conclusion

CO and  $\text{H}_2$  coadsorption on the  $\text{Fe}_5\text{C}_2(001)$ ,  $\text{Fe}_5\text{C}_2(110)$ , and  $\text{Fe}_5\text{C}_2(100)$  surfaces at various coverages has been computed at the density functional level of theory. For CO/ $\text{H}_2$  coadsorption on  $\text{Fe}_5\text{C}_2(001)$  at a coverage of  $\text{H}_2$  and CO of 1/6 ML, the stable surface species are 2-fold CO, 3-fold CO, 4-fold CO, H,  $\text{C}_3\text{H}$ ,  $\text{C}_3\text{H}_2$ ,  $\text{C}_3\text{HCO}$ , and  $\text{C}_3\text{H}_2\text{CO}$ . Surface  $\text{C}_3\text{H}$  and  $\text{C}_3\text{H}_2$  are formed

by H adsorption on surface carbon atoms, while ketenyl ( $\text{C}_3\text{HCO}$ ) and ketene ( $\text{C}_3\text{H}_2\text{CO}$ ) are formed by H adsorption or addition on the preformed ketenylidene ( $\text{C}_3\text{CO}$ ) from CO adsorption. With increased CO coverage (1/3 ML), the stable surface species are 2-fold CO, 3-fold CO, 4-fold CO, H,  $\text{C}_3\text{H}_2\text{CO}$ , and  $\text{C}_3\text{C}_2\text{O}_2$ . With increased  $\text{H}_2$  coverage (1/3 ML for  $\text{H}_2$ ), the stable surface species are 2-fold CO, H,  $\text{C}_3\text{H}$ ,  $\text{C}_3\text{H}_2$ , and  $\text{C}_3\text{H}_2\text{CO}$ .

For CO/ $\text{H}_2$  coadsorption on  $\text{Fe}_5\text{C}_2(110)$  with a coverage of 1/6 ML, the surface species are 2-fold CO, 4-fold CO, H, and  $\text{C}_3\text{H}_2\text{CO}$ . At the higher CO coverage (1/3 ML), top-CO, 2-fold CO, 3-fold CO, 4-fold CO, H, and  $\text{C}_3\text{H}$  are the stable surface species. At a higher  $\text{H}_2$  coverage (1/3 ML), 2-fold CO, H,  $\text{C}_3\text{H}$ , and  $\text{C}_3\text{H}_2\text{CO}$  are the stable surface species. These are similar to those on  $\text{Fe}_5\text{C}_2(001)$ .

At a coverage of 1/4 ML for both  $\text{H}_2$  and CO on  $\text{Fe}_5\text{C}_2(100)$ , the stable surface species are top-CO, 2-fold CO, and H. At coverages for  $\text{H}_2$  and CO of 1/4 and 1/2 ML, respectively, 2-fold CO and H are the stable surface species. At coverages for  $\text{H}_2$  and CO of 1/2 and 1/4 ML, respectively, top-CO, 2-fold CO, H, and  $\text{H}_2$  are the stable surface species. These results indicate the diversity of the atomic structures on the underlying  $\text{Fe}_5\text{C}_2$  surface sites.

**Acknowledgment.** This work was supported by the Chinese Academy of Science and the National Nature Foundation of China (20473111 and 20590360).

## References and Notes

- (1) Anderson, R. B. *The Fischer–Tropsch Reaction*; Academic Press: London, 1984.
- (2) (a) Datye, A. K.; Jin, Y. M.; Mansker, L.; Motjope, R. T.; Dlamini, T. H.; Coville, N. J. *Stud. Surf. Sci. Catal.* **2000**, *130B*, 1139. (b) Jin, Y. M.; Mansker, L.; Datye, A. K. *Prepr. Pap.—Am. Chem. Soc., Div. Pet. Chem.* **1999**, *44*, 97. (c) Bartholomew, C. H.; Stoker, M. W.; Mansker, L.; Datye, A. K. *Stud. Surf. Sci. Catal.* **1999**, *126*, 265. (d) Zhang, Y. Q.; O'Brien, R. J.; Davis, B. H.; Hamdeh, H. H. *Prepr. Pap.—Am. Chem. Soc., Div. Pet. Chem.* **1999**, *44*, 100. (e) Jin, Y. M.; Datye, A. K. *Stud. Surf. Sci. Catal.* **1998**, *119*, 209. (f) Davis, B. H. *Catal. Today* **2003**, *84*, 83. (g) O'Brien, R. J.; Xu, L. G.; Spicer, R. L.; Davis, B. H. *Energy Fuels* **1996**, *10*, 921. (h) Rao, K. R. P. M.; Huggins, F. E.; Mahajan, V.; Huffman, G. P.; Burkur, D. B.; Rao, V. U. S. *Hyperfine Interact.* **1994**, *93*, 1751.

- (3) Erley, W.; McBreen, P. H.; Ibach, H. *J. Catal.* **1983**, *84*, 229.
- (4) Rangelov, G.; Bischler, U.; Memmel, N.; Bertel, E.; Dose, V.; Pabst, M.; Rösch, N. *Surf. Sci.* **1992**, *273*, 61.
- (5) (a) Li, J.; Schiøtt, E.; Hoffmann, R.; Proserpio, D. M. *J. Phys. Chem.* **1990**, *94*, 1554. (b) Hoeft, J. T.; Polcik, M.; Sayago, D. I.; Kittel, M.; Terborg, R.; Toomes, R. L.; Robinson, J.; Woodruff, D. P.; Pascal, M.; Nisbet, G.; Lamont, C. L. *A. Surf. Sci.* **2003**, *540*, 441.
- (6) Bernasek, S. L.; Zappone, M.; Jiang, P. *Surf. Sci.* **1992**, *272*, 53.
- (7) (a) Merrill, P. B.; Madix, R. J. *Surf. Sci.* **1992**, *271*, 81. (b) Burke, M. L.; Madix, R. J. *Surf. Sci.* **1990**, *237*, 20.
- (8) Richter, L. J.; Germer, T. A.; Ho, W. *Surf. Sci.* **1988**, *195*, L182.
- (9) Getzlaff, M.; Bode, M.; Wiesendanger, R. *Appl. Surf. Sci.* **1999**, *142*, 428.
- (10) Rupprechter, G.; Morkel, M.; Freund, H.-J.; Hirschl, R. *Surf. Sci.* **2004**, *554*, 43.
- (11) Hahn, E.; Fricke, A.; Röder, H.; Kern, K. *Surf. Sci.* **1993**, *297*, 19.
- (12) Wang, H.; Tobin, R. G.; Lambert, D. K.; Fisher, G. B.; DiMaggio, C. L. *Surf. Sci.* **1995**, *330*, 173.
- (13) Henderson, M. A.; Yates, J. T., Jr. *Surf. Sci.* **1992**, *268*, 189.
- (14) Diemant, T.; Hager, T.; Hoster, H. E.; Rauscher, H.; Behm, R. J. *Surf. Sci.* **2003**, *541*, 137.
- (15) Becker, C.; Schröder, U.; Castro, G. R.; Schneider, U.; Busse, H.; Linke, R.; Wandelt, K. *Surf. Sci.* **1994**, *307*, 412.
- (16) (a) Koel, B. E.; Peebles, D. E.; White, J. M. *Surf. Sci.* **1981**, *107*, L367. (b) Peebles, H. C.; Peebles, D. E.; White, J. M. *Surf. Sci.* **1983**, *125*, L87. (c) Mitchell, G. E.; Gland, J. L.; White, J. M. *Surf. Sci.* **1983**, *131*, 167. (d) Peebles, D. E.; Peebles, H. C.; Belton, D. N.; White, J. M. *Surf. Sci.* **1983**, *134*, 46. (e) Westerlund, L.; Jönsson, L.; Anderson, S. *Surf. Sci.* **1988**, *199*, 109.
- (17) (a) Conrad, H.; Ertl, G.; Latta, E. E. *J. Catal.* **1974**, *35*, 363. (b) Kok, G. A.; Noordermeer, Nieuwenhuys, B. E. *Surf. Sci.* **1983**, *135*, 65.
- (18) Cao, D.-B.; Zhang, F.-Q.; Li, Y.-W.; Wang, J.-G.; Jiao, H. *J. Phys. Chem. B* **2005**, *109*, 833.
- (19) Stockwell, D. M.; Bianchi, D.; Bennett, C. O. *J. Catal.* **1988**, *113*, 13.
- (20) Loggenberg, P. M.; Carlton, L.; Copperthwaite, R. G.; Hutchings, G. J. *J. Chem. Soc., Chem. Commun.* **1987**, 541.
- (21) Cao, D.-B.; Zhang, F.-Q.; Li, Y.-W.; Jiao, H. *J. Phys. Chem. B* **2004**, *108*, 9094.
- (22) (a) Payne, M. C.; Allan, D. C.; Arias, T. A.; Joannopoulos, J. D. *Rev. Mod. Phys.* **1992**, *64*, 1045. (b) Milman, V.; Winkler, B.; White, J. A.; Pickard, C. J.; Payne, M. C.; Akhmataskaya, E. V.; Nobes, R. H. *Int. J. Quantum Chem.* **2000**, *77*, 895.
- (23) (a) Perdew, J. P.; Zunger, A. *Phys. Rev. B* **1981**, *23*, 5048. (b) Perdew, J. P.; Chevary, J. A.; Vosko, S. H.; Jackson, K. A.; Pederson, M. R.; Singh, D. J.; Fiolhais, C. *Phys. Rev. B* **1992**, *46*, 6671.
- (24) Vanderbilt, D. *Phys. Rev. B* **1990**, *41*, 7892.
- (25) Monkhorst, H. J.; Pack, J. D. *Phys. Rev. B* **1976**, *13*, 5188.
- (26) Louie, S. G.; Froyen, S.; Cohen, M. L. *Phys. Rev. B* **1982**, *26*, 1738.
- (27) (a) Nayak, S. K.; Nooijen, M.; Bernasek, S. L. *J. Phys. Chem. B* **2001**, *105*, 164. (b) Cheng, H. S.; Reiser, D. B.; Dean, S. W., Jr.; Baumert, K. *J. Phys. Chem. B* **2001**, *105*, 12547. (c) Ge, Q.; Jenkins, S. J.; King, D. A. *Chem. Phys. Lett.* **2000**, *327*, 125.
- (28) Le Caer, G.; Simon, A.; Lorenzo, A.; Genin, J. M. *Phys. Status Solidi A* **1971**, *6*, K97.
- (29) Immel, S. *Molarch<sup>+</sup>, MOlecular ARCHitecture Modeling Program V7.05*; Technical University of Darmstadt: Darmstadt, Germany, 2002.
- (30) Dry, M. E. *Catal. Today* **2002**, *71*, 227.
- (31) Moritz, W.; Imbühl, R.; Behm, R. J.; Ertl, G.; Matsushima, T. *J. Chem. Phys.* **1985**, *83*, 1959.
- (32) (a) Mordaunt, D. H.; Osborn, D. L.; Choi, H.; Bise, R. T.; Neumark, D. M. *J. Chem. Phys.* **1996**, *105*, 6078. (b) Brock, L. R.; Mischler, B.; Rohlfing, E. A.; Bise, R. T.; Neumark, D. M. *J. Chem. Phys.* **1997**, *107*, 665.
- (33) Lide, D. R., Ed. *CRC Handbook of Chemistry and Physics*, 3rd electronic ed.; CRC Press: Boca Raton, FL, 2000.
- (34) Tanimoto, M.; Kuchitsu, K.; Morino, Y. *Bull. Chem. Soc. Jpn.* **1970**, *43*, 2776.
- (35) Henderson, M. A.; Radloff, P. L.; White, J. M.; Mims, C. A. *J. Phys. Chem.* **1988**, *92*, 4111.
- (36) Matsumoto, H.; Bennett, C. O. *J. Catal.* **1978**, *53*, 331.
- (37) Biloen, P.; Helle, J. N.; Sachtler, W. M. H. *J. Catal.* **1979**, *58*, 95.
- (38) Kolis, J. W.; Holt, E. M.; Shriver, D. F. *J. Am. Chem. Soc.* **1983**, *105*, 7307.
- (39) Liu, Z.-P.; Hu, P. *J. Am. Chem. Soc.* **2002**, *124*, 11568.
- (40) Takeuchi, A.; Katzer, J. R. *J. Phys. Chem.* **1982**, *86*, 2438.
- (41) Chen, Y.-H.; Cao, D.-B.; Yang, J.; Li, Y.-W.; Wang, J. Jiao, H. *Chem. Phys. Lett.* **2004**, *400*, 35.
- (42) Blyholder, G.; Neff, L. D. *J. Catal.* **1963**, *2*, 138.
- (43) Blyholder, G.; Neff, L. D. *J. Phys. Chem.* **1962**, *66*, 1664.
- (44) Bertolini, J. C.; Imelik, B. *Surf. Sci.* **1979**, *80*, 586.